Additive Manufacturing xxx (xxxx) xxx

Contents lists available at ScienceDirect

Additive Manufacturing

journal homepage: www.elsevier.com/locate/addma

Corrosion performance of additively manufactured stainless steel parts: A review

Ali Hemmasian Ettefagh [a,*], Shengmin Guo [a], Jonathan Raush [b]

[a] Department of Mechanical & Industrial Engineering, Louisiana State University, Baton Rouge, LA, 70803, USA
[b] Department of Mechanical Engineering, University of Louisiana at Lafayette, Lafayette, LA 70503, USA

ARTICLE INFO

Keywords:
Corrosion
Additive manufacturing
Stainless steel
Laser powder bed fusion
Direct laser deposit

ABSTRACT

The application of additively manufactured (AM) stainless steel (SS) parts is rapidly emerging in a broad spectrum of industries. Laser powder bed fusion (LPBF) and direct laser deposition (DLD) are the main AM methods to fabricate a vast range of SSs like 316 L, AISI 420, 17-4 PH, 304 L, and AISI 4135. This article focuses on the corrosion performance of additively manufactured stainless steel parts made by LPBF and DLD. The passive film formation mechanisms and the corrosion performance of LPBF/DLD AM SS parts are discussed in comparison to their conventionally made counterparts. Microstructural features like porosity, inclusions, residual stress, surface roughness, elemental segregation, phases, and grain size distribution are elaborated thoroughly from the corrosion point of view, closely linked with the AM processing parameters. Generally, process parameters play an important role in the corrosion properties of AM parts by impacting the microstructural features. Assuming a proper set of parameters for the printing process, the overall corrosion performance of AM SS is better than its conventional counterparts. However, there are still controversies around some important aspects such as passive film structure, the nature of residual stress, post heat treatment processes, and grain size distribution and their impact on corrosion performance, which emphasizes the need for future studies in this area.

1. Introduction

Stainless steel (SS) alloys have significant uses in many industrial applications like aerospace, medical device, pipeline, automotive, and die and tool industries, in the form of austenitic, martensitic, ferritic, or austenoferritic (duplex) [1,2]. These categories are based on the microstructures of SS which are dictated by the chemical composition of the alloy and the manufacturing process [2–4]. The addition of elements such as chromium, nickel, carbon, molybdenum, copper, nitrogen, aluminum, sulfur, and selenium can modify the corrosion resistance, strength, ductility, machinability, and the stability of phases in SS alloys [1,5,6].

Different classes of SS such as precipitation hardening stainless steels [7], tool steels [8], austenitic stainless steels [9], and maraging steels [10] are frequently used in additive manufacturing (AM). Besides the general applications, SS can also be utilized for high hardness and strength purposes [11] due to its relatively high strength, low density, and outstanding corrosion performance. The main focus of this review paper is the corrosion resistance of SS, which is primarily attributed to the formation of a protective Cr_2O_3 passive film on the surface. This is possible when the chromium content is about 11 wt% or more [1,5,6].

Many types of SS have been additively manufactured and their mechanical or corrosion behaviors have been studied, Fig. 1-left. The chemical compositions of these alloys are presented in Table 1. The most studied SS alloy, 316 L, is an austenitic alloy widely used in industrial applications due to its high corrosion resistance along with acceptable mechanical properties [1,12]. Formation of a thin protective layer on the surface and the presence of molybdenum in its chemical composition are known to be the reason for its better performance against both general and localized corrosion attacks relative to other grades of austenitic SS such as 304 and 304 L [1,13–15]. In addition, the low carbon content of this alloy is beneficial for the welding process by decreasing carbide precipitation at grain boundaries [16]. Hence, 316 L is one of the few choices for the marine, medical and food industries where excellent anti-corrosion properties are needed [17]. AISI 420 is a martensitic SS, whose properties can be tailored by the heat treatment process [2,18]. Considering its good tensile strength, high hardness, and reasonable corrosion resistance, AISI 420 is also commonly used in industry. The final properties of this alloy are a function of the processing parameters. An anisotropic 3D structure has been noted for AM AISI 420

* Corresponding author.
E-mail address: ahemma3@lsu.edu (A. Hemmasian Ettefagh).

https://doi.org/10.1016/j.addma.2020.101689
Received 2 August 2020; Received in revised form 7 October 2020; Accepted 26 October 2020
Available online 4 November 2020

parts due to repeated heating and solidification cycles in melting-based AM processes [19,20]. Under the pre-hardened and tempered condition, a tensile strength of 700–930 MPa is reported [21]. Precipitation hardening (PH) SSs such as 17–4 PH, have recently gained interest in aerospace, nuclear, and marine applications for AM due to their duplex microstructure of combined martensite and austenite [22,23]. The tensile and impact strength, fracture toughness and corrosion resistance of those martensitic precipitation hardened SSs have been studied for high service temperatures up to 300 °C [7,24,25]. Another group of steels that has been evaluated for AM is High Strength Low Alloy Steels (HSLA) like AISI 4135 which, although often not categorized as SS, nevertheless has a wide range of applications despite their relatively poor corrosion performance [26,27]. However, it has been shown that adjusting the nickel content as an austenite forming element in the feedstock powder of the AM process can improve the corrosion resistance by affecting the microstructure of the alloy [28].

2. Additive manufacturing process

With the capability of producing near net shape and complex parts, additive manufacturing, also known as 3D printing, has found a growing demand in a wide range of industries and research topics [29–31]. The minimum waste of raw materials and rapid production of unique parts in small quantities are major benefits of AM [32,33]. In terms of corrosion performance, traditional methods may cause intergranular corrosion in SSs [34] and this is another reason for the rapid development of advanced technologies like AM. Metal AM is categorized into two main groups: the first group is known as powder bed fusion which itself includes two methods, laser powder bed fusion (LPBF) and electron beam melting (EBM). Direct laser deposition (DLD) is the second group of common metal AM processes [35,36]. Among these methods, LPBF and DLD are widely used for SS AM (Fig. 1-right) and will be discussed in detail.

LPBF, also known as selective laser melting (SLM), is the most widely applied method for the production of SS via AM due to relatively wide raw powder availability, remarkable flexibility in design, as well as cost and time savings [36]. The final part is produced layer-by-layer with computer-aided design (CAD) based control [37,38]. A focused laser beam (typically from a fiber laser doped with rare-earth elements) is utilized to selectively melt and fuse the successive layers until completing fabrication of a near-net-shape object, as shown schematically in Fig. 2-left [39,40]. Compared to traditional manufacturing methods, extreme local heating (up to 2500 °C), higher cooling rates (10^5–10^7 K/s), and re-melting of previous layers results in a novel microstructure of LPBF parts containing non-equilibrium phases with a large range of compositions, inclusions, and residual stress [41–43]. This condition also induces un-melted powder, porosities, the formation of dislocation cells, micro-cracks, and rough surfaces [44–46]. These metallurgical defects, along with the molten pool boundaries, can eventually lead to a sharp drop in plasticity and act as the preferred sites for localized corrosion [47–49]. Therefore, the quality of LPBF parts is the foremost challenge for using AM parts in various industries. It is acknowledged that process parameters including laser power, hatch spacing, scanning speed, layer thickness, and build direction dictate the final microstructure and service performance of the produced parts [43,50]. Moreover, a post-heat treatment process may be applied to reduce the mentioned defects and improve the service performance of the part as a result [49].

DLD is another additive manufacturing technology that is used to fabricate SS parts by a simultaneous supply of raw materials and energy to the build surface (Fig. 2-right) [51–53]. It is also known by many other names such as laser engineered net shaping (LENS), direct laser fabrication (DLF), direct metal deposition (DMD), direct light fabrication (DLF), laser metal deposition (LMD), laser deposition welding (LDW), powder fusion welding (PFW), laser powder deposition (LPD), direct energy deposition (DED), direct laser metal deposition (DLMD), or in some cases, the general title of "laser cladding" [2,33,43,51,54,55]. In this method, raw metal is fed to the device in the form of powder or wire and a laser source melts the feedstock and fabricates a near-net-shape part layer-by-layer based on a CAD design [45,51]. There is a precise control of the powder feed, laser power and other parameters in this method, and therefore, DLD can use a broad spectrum of raw materials. Several research papers are available showing a huge improvement in tensile and fatigue strength of DLD SS compared to the parts produced by traditional methods [56,57]. DLD can also be applied in surface engineering and additive repairing by tailoring the surface properties and/or composition based on their applications [58,59]. Cooling rate is a function of processing parameters and, based on experimental measurements, is estimated to be in the range of 10^3–10^5 K/s in DLD processes, which, when compared to LPBF, results in a coarser microstructure along with the possibility of more residual ferrite and a higher porosity level in the as-fabricated parts. These are important factors in functional properties and specifically, the corrosion behavior of the part [35,60–62]. Compared to LPBF, DLD employs a relatively higher energy density and for this reason and due to a larger melting pool, the cooling rate during DLD is significantly lower, but DLD solidification rates are still much faster than traditional casting methods [63–65].

3. Special applications of AM SS

The general application of AM SS parts is growing rapidly in industries such as aerospace, automotive, and marine based on the discussed advantages of this manufacturing method. For instance, many parts of a jet engine can be manufactured by AM in weeks as opposed to several months for traditional methods [67,68]. AM SS parts have been progressively used for some special environments that will be elaborated upon in this section with the focus on their corrosion performance. For these applications, the solution used for corrosion tests is different from the general application where a mixture of various concentrations of NaCl and water is used to simulate the working environment of the part ([69–72] to name a few). In all of these applications, AM is becoming increasingly popular by the day.

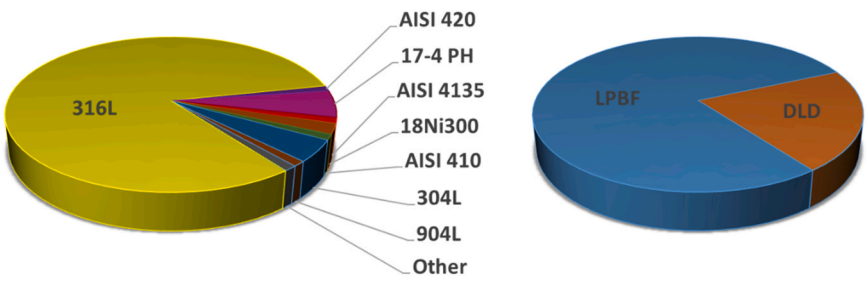

Fig. 1. (Left) Relative emphasis on types of AM SSs, (right) Relative emphasis on applied AM methods for SSs. The data were collected from over 300 research papers cited by this review article.

3.1. Bio applications

Due to its possessing excellent corrosion resistance with good mechanical properties, availability and reasonable cost, the application of SS, and specifically 316 L SS, has grown greatly for medical implants [73–76]. These applications include orthopedic bone fixation devices, orthodontic wires, plates and screws used in craniofacial applications, orthopedics for joint replacement and fracture repair, cardiovascular implants (stents, artificial valves), coronary and pulmonary stents, hip prosthesis, and artificial eardrums [77–79]. Electrochemical reactions of these parts inside the human body cause corrosion of the part. Corrosion in bio applications is an important issue, as it not only affects the lifetime and structural stability of the part itself but also causes inflammatory and anaphylactic reactions [80–82]. For instance, the release of Mo, Cr, and Ni ions from stents that are made of SS 316 L can cause immune reactions and limited inflammation (Fig. 3)[83]. All of these may affect the implantee quality of life and any failure may lead to severe pain and probable post-surgical operations [84–86]. For instance, Ni is one of the major alloying elements of 316 L SS. The release of Ni ions in the body results in severe inflammation in surrounding tissues and adverse cellular reactions due to its toxicity [86–88]. It also has been reported that the use of wrought 316 L SS causes the formation of a cytotoxic constituent through a set of corrosion reactions [89]. Generally, SSs are prone to localized corrosion that should be addressed in detail for bio applications. The formation of MnS inclusions in SS creates some regions with depleted chromium and these sites act as the initiation point of localized corrosion as a consequence of the heterogeneous structure of the oxide film [90,91]. A statistical study showed that after fracture (42%), corrosion is the second leading root cause of implant failures by frequency (24%), and before a vicious cycle of releasing small metal particles along with the implants (14%) [92]. Several approaches have been examined in order to increase the long-term stability of SS in the human body. Surface laser melting is proposed to selectively melt and dissolve MnS inclusions in the oxide surface followed by quenching to homogenize the protective layer [93–97]. Coating methods seem inefficient for this purpose considering the defective nature of coats and their mechanical instability [98]. Some researchers show that reinforcing the surface oxide by ion implantation can improve the corrosion resistance effectively, however, the high applied energy during this surface modification method worsens the surface topography which is also an important factor in implant failure [99–102]. Although a study shows that the passive film formed on AM SSs for bio applications is more stable with better barrier characteristics and has an improved cell adherence ability compared to traditional counterparts [79], improving the corrosion performance of AM SS to be used in the bio environment is still challenging and needs more research.

3.2. Nuclear industries

SSs and in particular, 316 L, are extensively used in the nuclear industry to manufacture both inside and outside parts of reactor pressure vessels in a relatively reduced time, cost, and supply chain, even employed during the plant's planned refueling outage [103–105]. The recent improvement in AM of 316 L SS results in the capability to produce near full density parts and this achievement has solved major concerns in using AM parts in nuclear facilities [106,107]. In nuclear reactors, SS is in contact with high-temperature water with a temperature of roughly 290 °C [108,109]. At this critical condition, a duplex oxide layer can be formed on the surface [110,111]. The outer layer mainly consists of either magnetite or hematite where the type of formed iron oxide depends on the electrochemical potential [112]. The inner oxide layer is the chief protective layer that prevents further diffusion of cations from the bulk through the surface layer. This layer is made of spinel oxides of iron, nickel, and chromium where the higher the latter, the more protective the oxide layer [113]. However, it is well known that stress corrosion cracking (SCC) is one of the major concerns of SSs in a nuclear plant, from their vulnerability to SCC while in high-temperature water (Fig. 4) [114]. The severity of SCC has been credited to the synergy of several parameters such as environmental chemistry, residual strain in the alloy, temperature, irradiation damage, surface condition, and electrochemical potential [115–121]. Based on these factors, and due to its lower SCC properties, it is not recommended to use AM 316 L SS in critical conditions without performing a recrystallization process and/or hot isostatic pressing (HIP) to further increase the density of the AM part and modify the microstructure. A study shows that the crack growth rate of AM samples after HIP and recrystallization processes is one tenth of the as-received AM SS 316 L samples [104]. However, engineering judgment is required to find an optimized balance between time/cost savings and the quality of the product [103,104]. SCC of SSs in high-temperature water has gained more attention in recent decades after several incidents involving intergranular stress corrosion cracking in reactors [122,123]. Two primary sources have been mentioned as the initiation sites for intergranular cracking: 1) the nucleation of chromium carbide in the grain boundaries along with the depletion of chromium in these regions as a result, and 2) increase in cracking susceptibility by the segregation of impurities such as nitrogen, sulfur, or phosphorus to the grain boundaries. Moreover, the presence of MnS inclusions are known to be responsible for transgranular cracking of SS in high-temperature water [115,123]. Additionally, extensive crack branching during SCC has been credited to the formation of Si-rich

Table 1
Chemical compositions of SSs (commonly processable by AM) in % wt.

Alloy	Cr	Ni	Mo	Mn	Si	P	C	S	W
316 L	16.13–18.74	10.0–13.6	2.0–2.8	< 2.3	< 1	< 0.12	< 0.03	< 0.03	< 0.04
	O	**Nb**	**Ti**	**Al**	**Cu**	**N**	**V**	**Co**	**Fe**
	< 0.05	< 0.01	< 0.01	< 0.01	< 0.20	< 0.15	< 0.05	< 0.13	Bal.
AISI 420	**Cr**	**Ni**	**Mo**	**Mn**	**Si**	**P**			
	12.26–12.30	< 0.17	< 0.03	1.1–1.2	0.11–0.50	0.015–0.023			
	C	**S**	**V**	**Co**	**Fe**				
	0.23–0.26	0.009–0.108	< 0.04	< 0.02	Bal.				
304 L	**Cr**	**Ni**	**Mo**	**Mn**	**Co**	**Nb**	**Si**		
	17.60–19.21	8.73–10.74	< 0.042	1.06–1.60	< 0.03	< 0.05	< 0.57		
	P	**C**	**S**	**O**	**N**	**Fe**			
	0.005–0.010	< 0.015	0.003–0.02	0.017–0.038	< 0.011	Bal.			
AISI 4136	**Cr**	**Ni**	**Mo**	**Mn**	**Si**				
	16.5	1.7	1	< 0.5	1.15				
	Si	**C**	**B**	**Fe**					
	1.15	< 0.18	1.25	Bal.					
17–4 PH	**Cr**	**Ni**	**Mo**	**Mn**	**Si**	**P**	**C**		
	15.19–16.02	4.12–4.54	0.025–0.230	0.22–0.53	0.17–0.33	0.013–0.022	0.017–0.047		
	S	**Ta**	**Nb**	**Cu**	**N**	**O**	**Fe**		
	< 0.002	< 0.001	0.23–0.29	3.21–3.95	0.023–0.036	0.014–0.068	Bal		

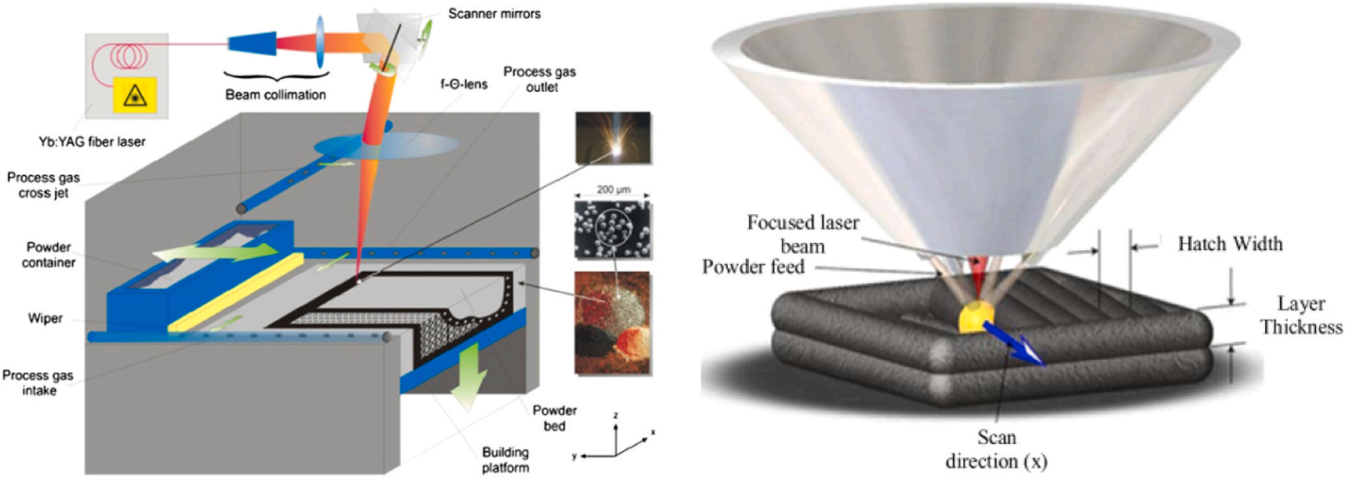

Fig. 2. Schematic view of (left) LPBF [66], and (right) DLD AM methods [60].

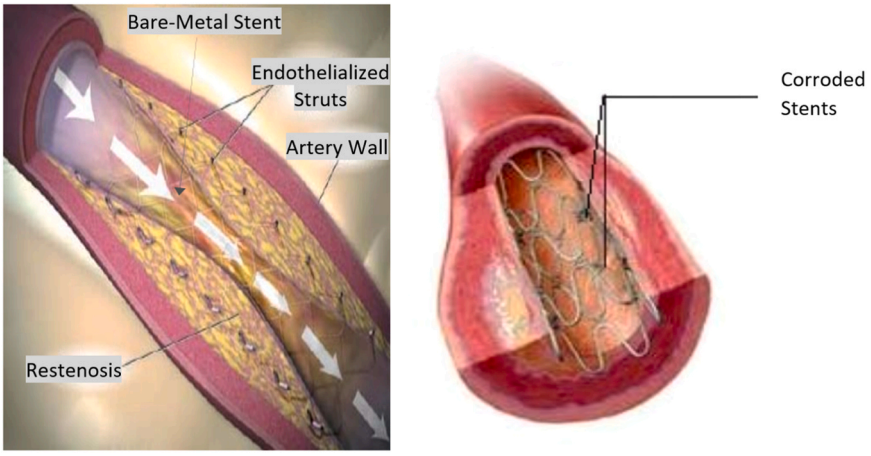

Fig. 3. Corrosion of stent made of SS 316 L [83].

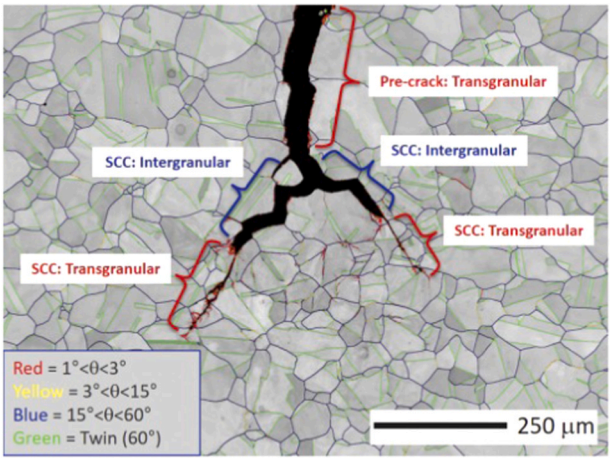

Fig. 4. EBSD SCC map of AM SS 316 L tested in high temperature water [104].

oxides along the grain boundaries. Therefore, controlling the amount of these elements either in the powder making process or AM build process is essential to reducing SCC susceptibility [109].

3.3. Bipolar plates in fuel cells

In a solid polymer fuel cell (SPFC) or a proton exchange membrane fuel cell (PEMFC), the bipolar plate serves several functions. The first role is to generate a flow field on the surface to provide reactant gases for the gas diffusion electrodes. Removing product water and making available a series electrical connection are other responsibilities of this multi-function component [124]. Currently, graphite is the most widely used material for this purpose despite its brittleness and lack of mechanical strength. Consequently, the plate needs to be thick enough to overcome these issues and this makes the cell bulky and heavy [125]. To find an alternative material for this purpose, the minimum requirements should be addressed. An ideal bipolar material possesses excellent corrosion performance, high electrical and thermal conductivity, high manufacturability, is chemically inert, and is low density with high mechanical strength [124–126]. Austenitic stainless steels possess most of these requirements along with a lower cost and the possibility of mass production compared to graphite plate. In addition, the high strength of SS allows the production of thin plates [49,124]. Therefore, SS are promising candidates for this application and several evaluations have been performed to assess their function as a bipolar plate.

From a corrosion point of view, it is stated that the degradation of bipolar plates is one of the key issues in the functionality of fuel cells that results in contamination of the system and decreases its conductivity. Two sources of corrosion attack have been mentioned in the literature:

1) the conducting membrane used in fuel cells is typically made from a perfluorinated sulfonic acid polymer which leaves the bipolar plate in a strong acid environment during its operation [127], 2) the oxidation reaction on the anode anodizes hydrogen and generates protons ($2H2 \rightarrow 4H^+ + 4e^-$). Hydrogen ions react with the oxygen on the cathode to form water molecules after passing through the membrane and reaching the cathode ($O_2 + 4H^+ + 4e^- \rightarrow 2H_2O$). Due to the presence of hydrogen on the anode surface and the moisture of the membrane, severe acidic conditions occur around the bipolar plate [125]. On the other hand, metal ions can poison the membrane of fuel cells [125,127]. All of these conditions show the importance of more corrosion-based research on using SS as an alternative material for bipolar plates, since the previous research does not provide satisfactory results [127–129]. The same path should be considered for AM SS for this application to assure the endurance of the part in service. For example, in the automotive industry, a fuel cell should last at least 3000–5000 h in service without evidence of corrosion attack [124].

3.4. Acidic media

Generally speaking, SSs are not recommended for highly acidic conditions, ascribed to the non-homogeneity (i.e. inclusions and chromium depleted zones) and instability of the passive film layer in such media [130–132]. These restraining parameters are more pronounced for AM parts and limit the application of AM SSs in acidic media. However, their performance in acidic conditions should be addressed since they might be exposed to low pH for some applications. For example, sulfur-oxidizing bacteria (SOB) may exist in the environment and produce sulfuric acid that causes microbial corrosion even in a non-acidic environment which is comparatively unpredictable and tremendously localized [133]. Breached pores and surface roughness of AM parts can increase such kinds of attacks by facilitating the metabolization of bacteria and consequently more by-produced sulfuric acid as a result. Another issue associated with AM SSs in a sulfuric acid environment is hydrogen embrittlement (HE) where hydrogen ions diffuse to the sample relatively easily to form brittle hydride and carbide participates [134–136]. The severity of HE is known to be directly related to structural defects acting as trapping sites for hydrogen. Therefore, AM parts are more susceptible to HE than traditional parts due to a comparatively higher density of pores and dislocations, as well as residual stresses that facilitate the diffusion of hydrogen into the structure [135,137].

Several studies have been conducted on the corrosion performance of AM SSs in acidic media. In this research, the porosity of the part is the most prominent factor by serving as crevice zones and should be noted. It has been reported that the stagnation of electrolyte inside the pores changes its chemistry toward a lower pH by hydrogen evolution and depassivation inside the pores [17,138,139]. In this condition, the outer areas act as cathodic sites along with severe anodic activities inside the pore, which leads to the initiation of corrosion attacks. Pores with all ranges of diameters expedite corrosion attacks. However, smaller pores (<10 μm) have the capability of passive film formation, which lowers, but not eliminates, the risk of localized corrosion attacks [49,70,140].

The grain size distribution of the AM part is another factor that is important in passive film formation and growth. To enhance the corrosion properties of AM SSs, grain refinement is one of the suggested processes to improve the growth of the passive layer in acidic media by decreasing the diffusion path length for chromium toward the surface to form a protective and homogeneous chromium oxide layer [141,142]. Severe plastic deformation (SPD), hydrostatic extrusion (HSE), and equal channel angular pressing (ECAP) are some of the reported methods to refine the grain size to sub-micrometer levels [143–145].

4. Passive film properties

Generally, the formation of a surface protective layer is known to be the reason for the extraordinary corrosion performance of SSs. Despite differences in reported compositions, several research papers confirm that the passive film of SSs consists of two layers of oxides and hydroxides of iron (III) and chromium (III) [146–148]. The majority of researchers believe that Fe can diffuse further outward since it has higher mobility compared to Cr, thus, the outer layer is mainly iron oxide and the inner layer is chromium oxide [149,150]. In some other papers, the duplex nature of the passive film is described as an outer layer of Cr hydroxide, and a mixture of Fe and Cr oxides as the inner layer enriched with Cr_2O_3 [151,152]. Unlike chromium compounds, iron oxide is not considered as a protective layer and has a slight decreasing effect on surface corrosion reactions [153,154]. Corrosion performance of SSs highly depends on the growth and stability of a passive film which is a function of several parameters such as corrosive media, alloy composition, microstructure, etc. [152]. For instance, in solutions with higher pH values, the formed passive layer is thicker and more stable due to the higher stability of iron oxide (outer layer) in alkaline solutions (Fig. 5). Quite the opposite, the inner chromium oxide layer is more resistive in acidic solutions where the passive film might be just a monolayer of chromium compounds at very low pH, which is identical for both AM samples and their conventional counterparts [142,151]. On another note, defects and inclusions in the passive film trigger localized corrosion attacks through several mechanisms like depleting a region of Cr or decreasing the re-passivation ability of the alloy [90,141,155]. The ability to recover the passive film after its removal is also important in erosion-corrosion studies [156].

In AM, considering the quite different production mechanism compared to traditional methods, process parameters play an important role in the passive film formation, stability, and self-repair capability. For example, in a study, the passive film of AM SS exhibited better barrier characteristics in extreme acidic media compared to traditionally made SS due to its finer grain structure, resulting in a lower corrosion rate as well as a higher breakdown potential [142]. Other studies report a thicker passive layer on AM samples in different media with a higher ratio of hydroxide content which shows the thickening has taken place in the outer layer of the passive film [76,153]. The thicker passive film of AM samples compared to their conventional counterparts is attributed to the higher dislocation density of the former, which are the preferred sites for the growth of passive film due to the higher lattice distortion and activation energy. Based on this hypothesis, it has been observed that the corrosion potential and the thickness of passive film both decreased after a post-heat-treatment process on as-fabricated AM parts [157]. Alternatively, using improper process parameters has a converse effect on the corrosion behavior due to the voids in the structure which worsens the stability of passive films [158]. Developing an unstable or

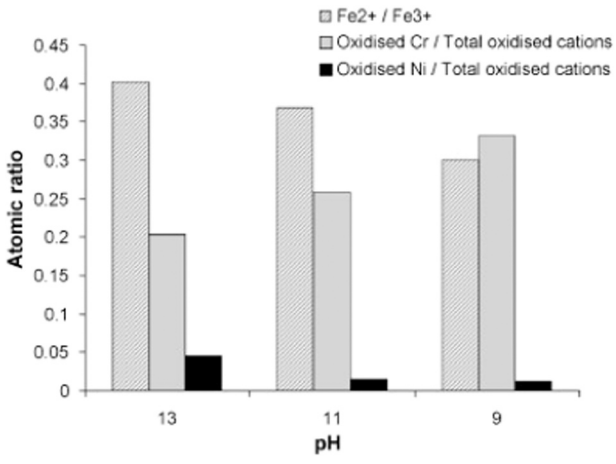

Fig. 5. Ion ratios in the passive film of SS 316 at different pH values, calculated from XPS spectra [150].

thin passive film on the surface will eventually lead to the formation of steady state pits and decrease the pitting potential [157]. It has also been demonstrated that the re-passivation ability of AM SS is relatively weaker than traditionally fabricated parts, attributed to the induced pores during the process. When the solution is trapped in these pores, chemistry changes of the solution inside the pore de-passivates and hinders the formation of the passive layer [140,159,160].

For bio applications, it is critically important to minimize the risk of AM SS implant corrosion by modifying and stabilizing the protective Cr_2O_3 layer on the metal substrate to postpone the corrosion reactions [161–163]. One of the suggested methods is thermal oxidation with optimum temperature and duration which accelerates the formation of iron and chromium oxides on the whole surface and even in protuberant areas of oxide film before contacting body tissues [164,165]. Too high temperatures or extended duration of soaking may lead to the breakdown of the chromium oxide layer and degrade the corrosion performance [84,153]. A study shows improved corrosion performance, both generally and localized, for AM SS 316 L in simulated body fluid (SBF) when processed at low power [88].

5. Metallurgical parameters affecting corrosion performance

In general, several metallurgical parameters such as phase distribution, microstructure, porosity, residual stress, surface roughness, etc. affect the corrosion performance as well as the mechanical behavior of metal parts [43,166,167]. In the AM process, these factors are determined by the printing process parameters including laser power, scanning speed, hatch spacing, layer thickness, and powder size [168,169]. On the other hand, localized heating and rapid solidification of metals during AM causes a different behavior compared to their traditionally manufactured counterparts, which emphasizes the necessity of broad studies on every aspect of AM to qualify these parts for industrial purposes [12,170]. SSs are exceptionally sensitive to process parameters [7,11]. For instance, there is evidence that lowering the formation of metallic droplets obstructs the preferred uniform spreading of the molten powder during laser melting (known as balling phenomena) in LPBF AM with non-optimized AM processing parameters [46,69,171,172]. It has also been shown that the number of dislocations in an AM SS is much higher than wrought SS due to fast cooling in the AM process which reduces the yield strength of AM samples [173]. In other literature, samples produced through the LPBF method with a higher energy density as a function of process parameters mostly demonstrated better performance compared to samples produced with lower energy density projecting the importance of optimization of the parameters [174]. In other words, optimization of parameters can eliminate some of the weak points of AM, i.e. modified microstructure, increased density [175,176].

In this section, seven key metallurgical characteristics that govern microstructure, passive film formation, re-passivation, and thus corrosion performance of AM SSs are described and the effects of process parameters on them are discussed in detail.

5.1. Porosity

Generally, pores are preferred sites for corrosion attack, especially pitting. AM as a powder-based manufacturing method is accompanied by the inevitable presence of pores in the produced parts, which can affect mechanical properties and corrosion performance [33,139,177,178]. Typically, pores appear either around the un-melted powder particles or due to trapped gas in the powder or melt pool during its initial processing, such as gas atomization or laser melting process, respectively. Elemental mapping of voids has revealed the presence of oxide powder and non-melted silicon in the pores of AM parts as confirmation of these sources [69]. Pores of AM parts can be categorized into two classes of regular (spherical) and irregular (non-spherical) pores (Fig. 6) [179,180]. Spherical pores form as a result of trapped gas during powder production and/or in the melting pool. This type of pore is relatively smaller than irregular pores. The geometry of regular-shaped pores and their inherent presence in the part, regardless of the printing processing parameters, have made them less important as a focus of corrosion studies of AM SS parts [4]. On the other hand, non-spherical pores form due to the un-melted powder particles which are the direct outcome of improper processing parameters [177]. As reported by many researchers, this class of pores, also called lack of fusion (LOF) pores, can considerably lower the density and play a significant role in facilitating both initiation (reaching the surface) and propagation (geometry and irregular shape) of pits, and the enrichment of aggressive ions at their corners due to their irregular shape [46,60,177,181,182]. In related studies, the breakdown potential (E_b) of the passive film was typically employed as an indication for passive film properties against localized corrosion attacks in the presence of pores. A lower E_b demonstrated a higher susceptibility to pitting associated with the presence of LOF pores compared to denser parts and to samples produced by traditional manufacturing methods. The overall qualitative

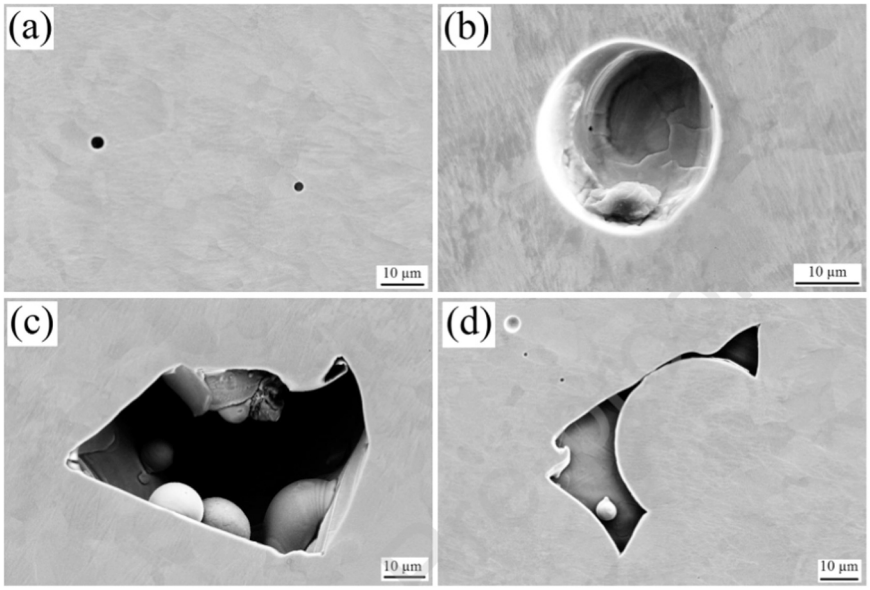

Fig. 6. (a, b) Spherical/regular-shaped, (c, d) non-spherical/irregular-shaped pores formed during additive manufacturing of SS 316 L by LPBF method [177].

results are almost identical in every environment including sulfuric and phosphoric acid, ferric chloride, as well as NaCl contained aqueous solutions [140,183].

Nevertheless, the level of porosity and the density of the part can be optimized to some extent by applying the right sets of printing parameters such as scanning speed and laser power, by affecting the heating and cooling rate of the melt pool [46,76,177]. For instance, too high a scanning speed (>1400 mm/s) or too low of laser power can dramatically accelerate the formation of LOF pores in AM SS caused by remaining un-melted powder. Too high of laser power, on the other hand, facilitates trapping of gasses in the printed part [4,69,177,184]. Several quantitative studies are available as evidence for this result. A study shows that a porosity level of above 2% with pore size up to 50 μm is the reason for poor corrosion performance of AM SS 316 L and 17–4 PH samples [17,70]. Similarly, a porosity level of 1.7% in AM SS leads to poor corrosion resistance compared to traditionally manufactured samples, even though the E_b values for both groups are in the same range [71]. Other studies report that samples with a density of higher than 99.1% have the highest E_b value compared to lower density levels and these values are almost identical to the traditionally fabricated samples with almost no effect on pitting potential [42,177,185,186]. Alternatively, a density level of lower than 99.1% results in unsatisfactory corrosion performance with an E_b value of 200 mV below traditional 316 L SS [177]. To validate the effect of porosity on corrosion performance of AM SSs, a comparison was made and confirmed the higher pitting potential of non-porous areas compared to porous regions of AM SS 304 L by greater than 200 mV. This finding endorses the role of pores in the pit initiation process [181]. A study on the metastable pitting characteristic of LPBF 316 L shows that by keeping the porosity level of AM SS 316 L in the range of 0.04–0.5%, pit initiation can be delayed remarkably compared to traditionally produced samples [4]. This behavior is claimed to be the result of the dissolution of MnS inclusions during rapid solidification in the AM process, which is known to be the main cause of pit initiation in SSs [187]. However, during polarization tests of AM and conventional SS 316 L, several current spikes have been detected at the high anodic potential for AM samples which is an indication of metastable pit formation. In other words, there is a pre-existing passive layer on the sidewalls of pores, but this protective layer is not stable enough and collapses at higher anodic potentials causing fluctuations on the anodic branch of the polarization curve. These fluctuations are more pronounced for the specimens with higher porosity levels [4,71,188]. Production processes and the quality of the feedstock can also affect the porosity level of the AM part [84,189]. Using powders with larger particles, irregular shapes, and higher contamination are all reported to increase the porosity level of AM SS parts [189]. Moreover, a study compares the final density of LPBF parts using either gas or water atomized 316 L SS powders and found utilizing water atomized powder results in a lower density due to higher oxygen content and lower packing density [190]. All of these parameters should be considered for quality purposes.

A more systematic optimization method for AM processing parameters to attain the densest possible AM SS parts is via laser energy density (LED), also known as volumetric energy density (VED), calculated by dividing laser energy by the product of scanning rate, hatch spacing and layer thickness [36,38,191]. A low level of LED causes non-spherical pores but high amounts of this parameter lead to the formation of spherical pores during the AM process [192,193]. Reports indicate that the densest SS 316 L samples with a porosity level of roughly 0.3% can be achieved by AM with a laser energy density of around 105 J/mm^3 [194]. However, despite this low level, porosities are not evenly distributed in the part. For instance, for 316 L SS produced by LPBF methods, the average porosity level was ~0.82% whereas the localized pore concentration in some regions were reported to be as high as 1.68% which may lead to anisotropic behavior of the AM part [195]. Taking everything into account, an AM SS with optimized processing parameters can demonstrate a comparable or even improved corrosion behavior compared to conventionally made SSs by keeping the porosity level as minimal as possible [12,33,196].

5.2. Inclusions

Austenitic SSs such as 316 L and 304 L are typically vulnerable to pitting corrosion due to the presence of unwanted inclusions as the second phase in the austenite matrix. Manganese sulfide (MnS) is the most prominent, and has a significant role in the corrosion performance of SSs depending on their density, composition, and size. The elimination or size control of MnS can be presumed as a corrosion inhibition method of SSs [90,91,197–200]. During the steelmaking process, Mn is added to form MnS and neutralize the negative effect of FeS formation. In other words, MnS is thermodynamically more stable and has a higher melting point compared to FeS, and its formation eliminates the presence of low melt FeS along grain boundaries in the steel structure which is the leading cause of cracking problems during hot rolling [201]. However, it is theorized that there is a drop in chromium content of the alloy in the areas surrounding MnS inclusions, and this Cr depleted region together with the inclusion itself have a lower Cr content than the critical value for passive layer formation which leads to localized corrosion vulnerability [38,90,131,198]. During the pit initiation process, elemental and ionic sulfur (S, S^{2-}, HS^-, $S_2O_3^{2-}$) are formed as a result of MnS oxidation which provides an inappropriate environment for the re-passivation process and pits propagate as a result [90,202–205].

On this basis, considering the rapid solidification associated with the AM process, much research has reported that no, or at least much smaller, MnS inclusions and Cr depletion zones in the matrix form, which causes a substantial increase in the pitting potential of AM SSs -by roughly 300 mV in different corrosive media [46,69,94,155,181,187,206]. However, in traditional manufacturing methods, the cooling rate is relatively lower, providing enough time for Mn and S to diffuse and form deleterious MnS inclusions [104,109]. The increase in pitting resistance of AM parts is also attributed to the change in chemistry, size, and shape of inclusions after the AM process. Several studies show the formation of nanoscale oxide inclusions enriched of Mn, Si, Al, Cr, N, and O (Fig. 7) which have no negative effect or even improve corrosion performance [155,181,187,207–210]. The size of inclusions after the AM process is in the range of 5–200 nm as opposed to their conventional counterparts with inclusions in the size range of 2–4 μm which is 1–3 orders of magnitude larger [76,181,187]. This range of nano-inclusion size is reported to exist in both LPBF and DLD methods of AM and are too small to initiate pitting corrosion in AM samples [9,206,207,211]. Also, the shape of the inclusions after the AM process is reported to be spherical versus irregular shapes in conventionally fabricated parts [187].

Since post-heat-treatment is an inevitable process in many industrial

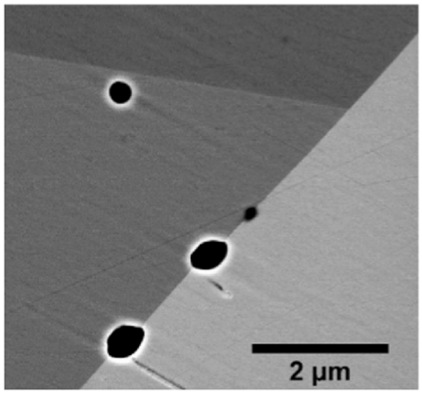

Fig. 7. Back-scattered electron image showing the formation of oxide inclusions in recrystallized AM SS 316 L [109].

applications of AM parts, it is important to understand the effect of heat treatment on the preformed inclusions during the AM process. After the post-heat-treatment process, the inclusions become smaller in size, and from the chemical composition point of view, the elements with lower melting points such as Al diffuse to the matrix and change to the composition of nano-inclusions [49,157]. The lingering inclusions in a heat-treated AM part can be categorized into three classes: (1) Manganese silicate inclusions formed in the as-fabricated samples which still exist after a heat treatment process in the temperature range of 900–1000 °C with a duration of 15–60 min; (2) Heat treatment at temperatures of 1100–1200 °C will result in the formation of irregular manganese chromite inclusions from the manganese silicate inclusions; and (3) Harmful MnS inclusions (pitting initiators) which are formed in the same heat treatment condition as type (2) and should be acknowledged as the main reason for dramatic decreases of corrosion resistance after heat treatment processes on AM SS parts at temperatures above 1000 °C. At this high temperature, the non-equilibrium state of the as-fabricated structure has enough time to move toward the equilibrium state by forming MnS from saturated Mn and S in the matrix [72].

5.3. Residual stress

Heating and cooling regimes during melting of the top layer and re-melting of underlying layers in the AM process causes anisotropic residual stress in different regions of the produced part where in some places, it may exceed the yield strength of the material, distort the part, and affect both mechanical and corrosion performance [212,213]. Alternatively stated, rapid heating, fast solidification, and thermal expansion cause elastic strain and local distortion of the lattice which develops residual stress in either tensile or compressive forms [214]. The considerable thermal gradient (Fig. 8-left) which enhances distortion within the AM part is one of the impelling parameters on the magnitude of residual stress along with several others such as build direction, yield strength, process parameters, and shape of the part. All of these parameters result in a more complicated behavior of residual stress in AM parts compared to parts that evolve through the traditional manufacturing methods [213,215–218].

Two models have been proposed to hypothesize the source of residual stress during AM. According to the temperature gradient mechanism (TGM) model, a laser source with high energy density heats a small area of the feedstock. This area tends to expand due to the input heat, but this thermal expansion has been restricted by the neighboring areas with lower temperatures, which induces a compressive stress during the heating stage. Conversely, during the cooling stage, the same area tends to shrink after the removal of the heat source, however, previously formed plastic strain limits the shrinkage and causes tensile stress in the location [216]. The cool-down phase model is another approach to explain the generation of residual stress in AM parts. Based on this model, which is founded on the layer-by-layer nature of fabrication, re-melting and re-solidification occur in underneath layers as well as the top layer, and each layer tends to shrink after cooling down. Because of this thermal cycle, and limited in shrinkage with its sublayer, tensile stress is developed in the layers [213].

Residual stress can be classified length scale-wise into three categories (Fig. 8-right): Type I (macroscale), Type II (microscale, anisotropic properties on grain-scale), and Type III (nanoscale, dislocations or vacancies) [219]. Although almost all of the studies on the effects of residual stress on the properties of AM parts ignore the small effects of types II and III on the overall residual stress in the structure, a few research papers demonstrate qualitatively that a post-heat-treatment on as-fabricated AM SS can reduce the dislocation density and type III of residual stress as a result [220,221]. The measurement of local residual stress in a part is difficult and requires some advanced methods involving advanced sample preparation and data analysis with X-ray or neutron based techniques. However, some simpler optical-based measurement methods are now employed by industries to analyze residual stress distribution and structural integrity of AM parts. The hole-drilling method (HDM) accompanied by electronic speckle pattern interferometry (ESPI) is a common method for this purpose [214,217,222–225].

The nature of residual stress in AM SSs is quite complex and controversial in different studies. Some studies show that the compressive stress in the part induced during the manufacturing process may increase the corrosion resistance by lowering the passive current density due to forming a denser passive film on AM SSs [226]. With this assumption, post-heat-treatment may be harmful to corrosion performance by eliminating the compressive residual stress [187]. Some studies even suggest introducing the compressive stress externally on the surface of the manufactured part to slightly enhance the corrosion performance [227–230]. This hypothesis is based on the role of compressive stress on lowering the point defect concentration of the passive film which increases the resistance to pit initiation and decreases the passive film growth rate [12].

Generally, including the role of residual stress in distortion of the AM part, which is more noticeable in thin-walled designs [225], residual stress is believed to accelerate both corrosion attack and stress corrosion cracking (SCC) [231–234]. A study claims that the regions under tensile stress and compressive stress form a micro galvanic couple where the former acts as anode and the latter as the cathode. This galvanic couple region has been mentioned as the primary pit initiation sites of the part [235,236]. In addition, delamination of the layers and initiation and growth of cracks have been mentioned as a direct result of residual stress, which is specifically important to the study of SCC of AM SSs [17,104]. However, countless stress/strain conditions on the surface of AM parts makes it very difficult to evaluate the SCC of these parts using modeling of residual stress formation [237]. In addition, it has been shown that the change of residual stress grows with depth of the printed part and this means the underneath layers are favored for the initiation of SCC [217].

As mentioned before, there are several distinct compressive/tensile sites on the AM surface, which makes this topic more complicated [237].

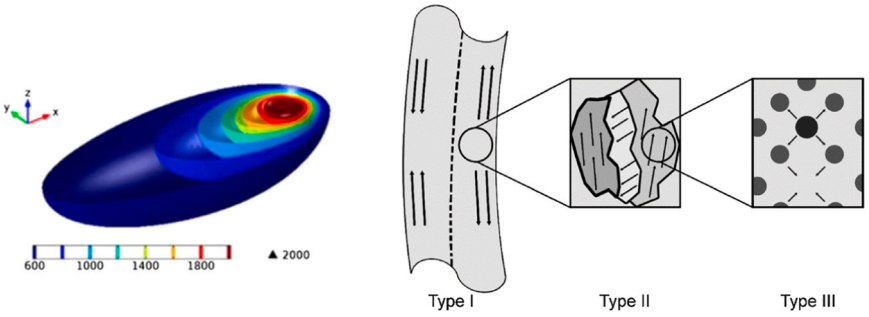

Fig. 8. (left) Temperature contour during additive manufacturing of SS 316 L shows a temperature gradient of ~2000 K on the surface [215], (right) different classifications of residual stress based on the length scale, type I: macroscale, type II: microscale caused by misalignment of grains, and type III: nanoscale caused by substitutional atoms [218].

Taking into account the complex impact of residual stress on the properties of the materials, it is almost inevitable to seek a remedy for decreasing this parameter in AM parts for industrial applications. Some methods are applied to reduce the residual stress in AM SSs. The most common is to preheat the feedstock and substrate material to decrease the thermal gradient within the part [238–240]. Moreover, applying severe plastic deformation (SPD) on as-fabricated parts as a post processing procedure is presented to be an effective method for improving material properties by producing an ultra-fine grained microstructure [38]. Post annealing is another typical remedy to decrease the residual stress of printed parts [196,241]. However, in all of these methods, the formation of a secondary phase may act as a new source of residual stress which should be addressed [237].

5.4. Surface roughness

Surface roughness as an inherent characteristic of AM parts is one of the key parameters in determining their corrosion behavior since a rougher surface accelerates electrochemical reactions between the surface and environment leading to both general and localized corrosion [242,243]. The surface roughness of AM parts is quite higher than other traditional manufacturing methods and highly depends on the laser energy density (Fig. 9). For example, research shows a roughness of 10–30 μm for AM LPBF parts as opposed to ~1 μm for parts produced by milling [244]. Four main reasons have been mentioned as the sources of a rough surface on as-fabricated parts [46, 245–247]:

1) Evaporation: an unstable and irregular melt pool during the AM process is attributed to the produced gasses during the powder melting along with the Marangoni force which destabilizes the melt flow and increases both surface roughness and porosity [248–250]. Less gas expansion is reported for thinner powder layers. However, choosing a smaller powder layer thickness extends the production time which should be taken into account [251,252].
2) Balling phenomena: low laser power cannot deliver sufficient energy to melt the powder particles completely. Consequently, the adhesion of solid particles to the surface increases the surface roughness [171,253]. Increasing the heat input by using higher laser power can be assumed as a remedy for this issue. In addition, higher heat input increases the wettability of the melt via the keyhole effect and enhances the interlayer connection by flattening the melt pool. This phenomenon also relieves the surface tension of the melt and reduces the balling phenomena and the eventual surface roughness as a result [172,254]. However, an optimized heat input should be applied since too high a heat input can be harmful to surface roughness by agitating the melt pool and growing recoil pressure [246]. Another reason for balling phenomena is the size of the initial powders. As the laser spot diameter is usually 50–100 μm, it is difficult to melt powder particles with a diameter of more than 100 μm which leaves a negative effect on the surface roughness [255,256]. Another study shows that the accumulated heat during AM of a thin-walled object increases the adhesion of partially melted particles to the surface and deteriorates the final surface finish [246].
3) Staircase effect: an additively manufactured part is created by stacking several 2D layers on top of each other to form a 3D object. However, a geometric difference is expected between theory (CAD design) and the actual printed part [257]. This difference is attributed to the layer-by-layer build up during AM and is known as the staircase or stair-stepping effect, which is more pronounced for inclined surfaces [258]. Using initial powders with a smaller diameter is proposed to diminish the staircase effect along with a decreasing layer thickness [45,257].
4) Facing orientation: several pieces of research literature express a difference in the surface roughness for upward and downward facing surfaces with different angles of inclination. Results show that upward-facing surfaces have a lower surface roughness. This is likely from filling of the gaps by the particles during the manufacturing of upward-facing surfaces [250,259,260].

5.5. Alloying elements and elemental segregation

It is well known that the outstanding corrosion performance of SSs is principally attributed to the presence of at least 11 wt% Cr as an alloying element that forms a protective layer of chromium oxide on the surface

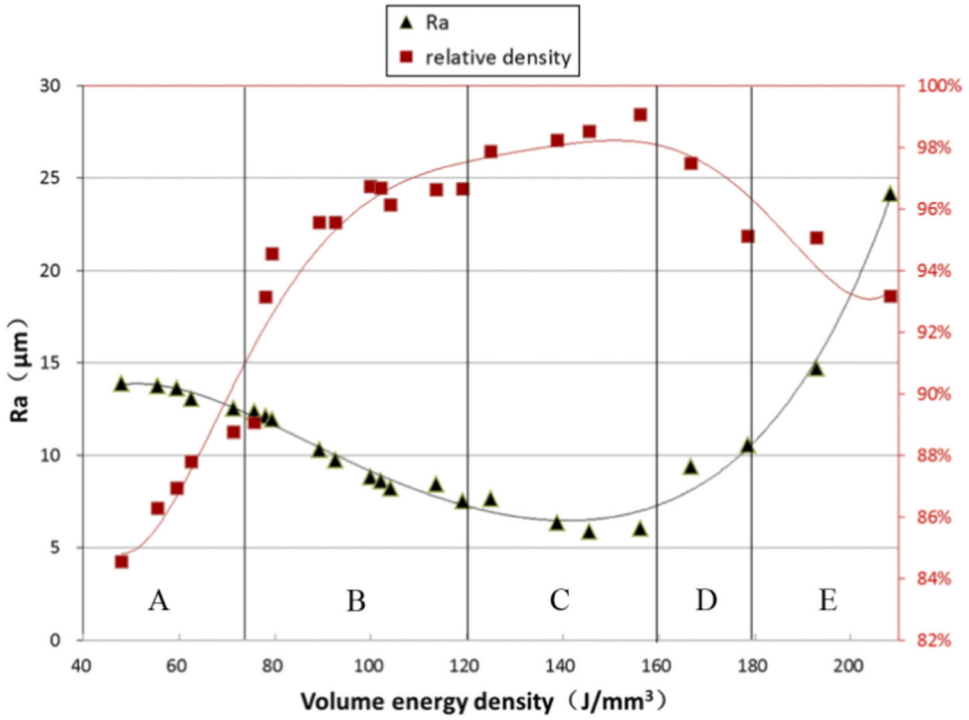

Fig. 9. Dependence of surface roughness to laser energy density for as-fabricated SS 316 L [244].

[261,262]. However, the role of other elements is not negligible in both mechanical and corrosion properties of AM SSs. Ni is generally known as an austenite stabilizer element by lowering the austenite/ferrite or martensite transformation temperature to sub-zero temperatures [263]. It also affects AM SS properties such as cracking susceptibility, wear resistance, microhardness, microstructure, and corrosion and oxidation resistance. For some types of SSs like 35CrMO, poor corrosion resistance limits its application in industry. It has been reported that by optimization of nickel content in such alloys, it is possible to improve corrosion properties while maintaining its significant mechanical behavior. This enhancement is ascribed to the formation of austenite instead of ferrite as the constituent phase due to the change of the solidification model as a result of increasing Ni content. Quantitatively, adding roughly 10 wt% of Ni to the initial composition of 35CrMo SS suppresses the anodic dissolution of SS by dropping the corrosion rate by an order of magnitude along with an increase of ~220 mV in corrosion potential for the as-fabricated sample [28]. There are, however, some limitations associated with nickel such as its high cost and allergic reactions in the case of bio-applications [263]. For this reason, developing low-nickel or nickel-free SS powders for AM is a new subject of interest. Nitrogen, as an interstitial element of SSs, causes a more homogenous distribution of other alloying elements and decreases the tendency of forming Cr clusters in the structure. Therefore, by strengthening the solid solution and improving short-range order, nitrogen is recognized as a strong austenite former in SSs [264]. With the presence of nitrogen in the alloy composition, the development of Cr clusters is prevented, creating a more efficient passive layer of Cr_2O_3 on the top layer, and improving intercrystalline, pitting, and crevice corrosion resistance as a result [265–267]. The common method for adding nitrogen to the initial powder of the AM process with a higher amount than its solubility range is to first add manganese to increase the solubility of nitrogen and lower the nickel content. The next step is to melt SS under a nitrogen atmosphere where nitrogen atoms are absorbed into the melt [268,269]. However, it should be noted that excessive nitrogen causes the formation of CrN and gas pores during the AM process. Research demonstrates that adding 0.3 wt% of N with this method can improve the stability of austenite in modified AM SS 316 L [270].

Oxygen may be introduced to the feedstock powder in the powder making process. This preexisting oxygen transforms to surface oxides on powder particle surfaces during the AM process and considerably lowers the pitting potential of AM SSs [70]. C and Mo are also important alloying elements in the composition of SSs from a corrosion point of view. The formation of carbides and their precipitation at grain boundaries causes intergranular corrosion. Hence, the amount of this element should be kept low (~0.03 wt%) [61,271]. The presence of Mo in the alloy composition is essential for the formation of the passive film and improves pitting resistance [1,13]. Studies show that Mo forms some oxyanions such as molybdate in the passive film and these anions act as corrosion inhibitors [73,272]. Moreover, an intermetallic layer of Mo-Ni is formed beneath the top passive layer which increases the protection and blocks the inward diffusion of aggressive ions like Cl [273].

The high energy associated with the AM process causes the vaporization of some powder particles or coverts them into soot, and also cause microsegregation in the elemental distribution of the printed part [274,275]. A study shows that in an AM SS 316 L, Cr and Ni contents vary in the range of 9–15% and 5–10%, respectively, while some regions with no Mo content have been detected which confirms the existence of areas with the subcritical amount of key alloying elements [276]. Considering the mentioned role of each element in the corrosion performance of AM SSs, this segregation leads to the spatially heterogeneous composition of SSs and impacts their corrosion behavior [73]. For instance, lower nickel and chromium contents are reported at the center of the AM part due to its relatively higher built-up energy during the process. Furthermore, the regions with lower Mo content have a different passive formation mechanism, which makes it less protective locally and increases the passive current density. This increase is as high as an order of magnitude in acid solutions compared to traditionally fabricated SSs [73]. Therefore, applying any redistribution process such as heat treatment on AM parts might considerably influence their corrosion behavior.

5.6. Grain size and shape

Generally, depending on the corrosive media, grain size affects the corrosion performance of SSs. For instance, in acid media, grain size below 2 μm is reported to increase the general corrosion rate of SS 304 due to an unstable passive film at the grain boundaries [277]. In contrast, the nano-scale grain size range purportedly improves corrosion performance [278]. However, some reports show the loss of passive layer protection on the surface of nano-crystallized SS 316 due to the increasing number of active sites for corrosion attack [279]. The effect of grain size on the corrosion performance of AM SSs is also controversial considering quite contradictory results reported in the literature. EBSD analysis shows that AM SS grains are more irregular and elongated perpendicular to the scanning direction with a large size range versus regular polygonal grains of traditionally fabricated samples with a narrow range of size, which is attributed to the much lower cooling rate of conventional manufacturing methods. Specifically for AM processes, some of the researchers demonstrate the existence of sub-grains with sizes of 0.5–1 μm inside each grain in the as-fabricated structure (Fig. 10) with an elevated concentration of Mo and dislocation density at sub-grain boundaries, which increases the reactivity of the surface as well as the risk of intergranular corrosion [49,73,88,207,210]. Moreover, unlike LPBF with complete austenite phases, for the DLD method, sub-grain boundaries were found to be enriched of Cr and Mo and almost depleted of Ni. There is an indication of the formation of intercellular delta ferrite on the sub-grain boundaries of AM SS 316 L which is one of the downsides of DLD over LPBF considering its lower cooling rate during the process [33,280–282]. It is stated that the effect of AM processing parameters on the average grain size is relatively insignificant [69,73], however, a strong relation between laser energy density and scanning strategy with resulting sub-grain structure has been reported [2,208]. A comparison between the corrosion rate of AM samples and their conventional counterparts shows that the degradation of corrosion performance after the AM process not only is the outcome of sample porosity but also because of the grain structure of as-fabricated samples [73,283]. On the contrary, others believe that this super high density of sub-grain boundaries of as-fabricated SSs acts as the preferred sites for passive film nucleation, resulting in a more protective surface layer [46,76,284].

The shape of grains is especially important in the SCC performance of AM SSs where the elongated grains cause an anisotropic behavior against crack growth. Considering grain elongation in the build direction, a crack faces more grain boundaries perpendicular to the build direction, resulting in a slower propagation rate [286–290]. Alternatively, elongated grains have been known as a source of localized corrosion attacks [73].

Grain refinement processes reportedly improve the corrosion and mechanical performance of stainless steel [291–294]. Modifying the surface texture to nano-scaled grains or ultra-fine grains decreases the chromium diffusion path to the surface and thickens the formed protective film in a corrosive media by promoting passive film formation [295]. Commonly, severe plastic deformation (SPD) methods have been applied as a post-treatment on as-received AM SSs to decrease the grain size to the ultrafine (0.1–1 μm) or even nano-scale range [296,297]. Several SPD techniques such as accumulated roll bonding (ARB) and equal channel angular processing (ECAP) are being tested on AM SSs to achieve this goal. However, high-pressure torsion (HPT) is the most popular method, refining the grain structure uniformly down to below the 50 nm range and eliminating scan tracks by imposing an extreme torsional strain on a sample [298–302]. Among several advantages of

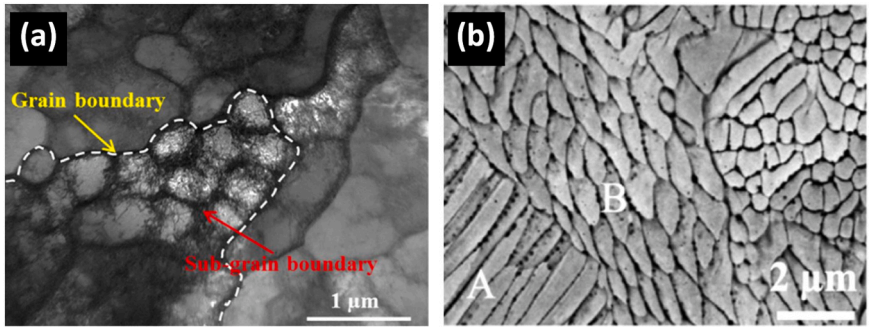

Fig. 10. (a) TEM image [76] (b) SEM image [285] of AM SS 316 L showing grain and sub-grain boundaries inside them. A and B represent two different grains.

HPT over other post-treatment SPD methods, the most important to achieve higher corrosion resistance in AM SSs are obtaining much smaller grains, higher efficiency, and producing grain boundaries with higher misorientation angles [61,303]. Recrystallization heat treatment is another method for refining grains by removing melt pool boundaries, sub-grain boundaries, and dislocations of as-fabricated SSs to improve their corrosion performance [49,185]. It is reported that holding samples fabricated from SS 316 L and SS 304 L at 1060 °C for 30 min followed by furnace cooling partially recrystallizes the as-fabricated structure and generates more grains along the closed packed direction (110) which is known to have higher pitting resistance [49,304]. Additionally, recrystallization decreases the crack growth rate and lowers the risk of SCC as a result of the elimination of the microstructural anisotropy [305]. However, a post-heat-treatment process should be performed cautiously at temperatures above 1000 °C since some research suggests lower corrosion resistance of recrystallized samples compared to as-fabricated ones due to the elimination of sub-grain boundaries and the precipitation of inclusions. In other words, sub-grain boundaries act as nucleation sites for passive film and their elimination leads to a thinner protective layer on the surface [185,284,306,307]. On the other hand, heat-treatment at temperatures below 1000 °C not only retains sub-grain boundaries but also transforms the dislocation walls to sub-grain boundaries, which along with stress-relieving and eliminating melt pool boundaries (instead of recrystallization), are believed to be beneficial for corrosion performance [185,196].

5.7. Phases

Generally speaking, despite the presence of "austenite" in the title of austenitic SSs, according to the Fe–Cr–Ni phase diagram, equilibrium phases at room temperature are listed as σ, δ-ferrite and carbides [308]. This means that applying an improperly designed thermal regime during either manufacturing or post-processing causes the formation of the mentioned unwanted phases, which are in contrast to the better corrosion performance of a fully austenitic microstructure. Among the mentioned unwanted phases, σ has the most detrimental effect on the corrosion behavior of SS by significantly decreasing the Cr amount on its interface and reducing pitting resistance and ductility of SSs as an intermetallic phase with tetragonal crystal structure [309–311]. In all AM manufacturing methods, phases are vastly different from the equilibrium phases considering the non-equilibrium nature of the process. However, as-fabricated phases may be different for LPBF and DLD methods. For LPBF, while the cooling rate is much faster than equilibrium conditions, the formation of unwanted phases is unlikely and a fully austenitic microstructure with cellular-dendritic substructures can be achieved by selecting the proper printing parameters [76,312]. The core of these austenite dendrites contains a lower amount of Cr and Ni compared to the initial composition which can act as initiation sites for corrosion attacks in some solutions such as ferric chloride [313]. However, a general evaluation of the sole effect of the microstructure of AM SSs by the LPBF method shows a minor role of unwanted phases in corrosion performance so that it can be neglected [181]. For the DLD method, taking into account its comparatively lower cooling rate than LPBF, the formation of unwanted phases along the sub-grain boundaries is more probable during manufacturing. Intracellular δ-ferrite has been reported to be formed considerably for different types of AM SSs through the DLD method [33,62,314–316]. For this reason, performing a proper post-heat-treatment is unavoidable in the case of a high content of unwanted phases to ensure a fully austenitic microstructure. It is claimed that solution annealing in the temperature range of 1040–1120 °C followed by water quenching can dissolve unwanted phases into the austenite matrix [311,317]. However, despite some reports about the effect of solution annealing on the improvement of SCC resistance and mechanical properties of AM SSs for high-temperature applications [104,318–320], heat-treatment might have some negative effects on the corrosion behavior as described in the last section.

6. Knowledge gaps and prospects

Although there have been many studies about the corrosion behavior of AM SSs, there still exists a lack of conclusive information in some cases, which indicates the necessity for future work in this area. Below are some of the important gaps that the current efforts have not addressed or for which there are controversies regarding their outcomes.

- The studies focused on AM processes involving several variables such as process parameters, alloy composition, test method, electrolyte, pH, and temperature, which makes a general cross-paper study and comparison difficult. A standard test method for corrosion performance of AM alloys can be provided by related organizations which facilitates the application of AM components in industry.
- The main source of different metallurgical properties of AM parts is printing processing parameters. An optimized set of parameters significantly affect the corrosion performance in different media. However, there is a lack of systematic analysis to introduce the optimum set for each alloy in a certain environment.
- There is not a general agreement on the source of residual stress and its effect on corrosion performance. The same controversy exists relative to the passive film formation mechanism on AM SSs parts and the role of microstructure, grain size and structure on the passive layer.
- There is also needed clarity on the best use of heat treatment since there can be both positive (densification, grain refinement) and negative (reduction of dislocation density, elimination of sub-grain boundaries, precipitation of inclusions) effects on the corrosion performance.
- Currently, all of the research on AM SS is limited to the alloys available on the commercial market. However, considering the distinct conditions during AM processes like high energy, rapid cooling rates, and micro-segregation, designing new SSs tailored especially for AM is an interesting topic.

- There is a lack of information about the long term exposure of AM SSs in industrial applications.

7. Conclusion

This review paper summarized the assessments on additively manufactured stainless steel parts with the focus on corrosion performance in a vast range of applications including biomedical, nuclear, and fuel cell industries, which require a higher degree of consideration regarding corrosion. Pros and cons of LPBF and DLD as the leading AM methods to manufacture SS parts were discussed and compared with conventionally manufactured counterparts. The main difference between the two methods is the relatively faster cooling rate during LPBF which results in fewer inclusions and unwanted phases. Moreover, passive film properties and its formation mechanism were elaborated in detail with the effect of process parameters on its quality. The core part of the paper is a systematic review of the microstructural features of AM SS parts such as porosity level, precipitation of inclusions, residual stress, surface roughness, chemical composition, and elemental segregation, grain size, and phases. In each section, the source of each feature and the effect of AM processing parameters were discussed and its role in the corrosion performance was evaluated.

- The level of porosity and the density of the part can be optimized by applying the right sets of printing parameters. AM SS parts with porosity levels below 1% showed almost identical, or in some cases better, corrosion properties compared to the traditionally made samples. However, current spikes in the anodic branch of polarization curves confirm metastable pit formation due to the presence of pores in the structure.
- Due to the rapid solidification during AM, MnS inclusions and Cr depletion zone sizes are much smaller than in traditionally made samples (nano-scale vs. micro-scale) regardless of the process parameters, resulting in a higher pitting resistance of AM SS parts. A post-heat-treatment at temperatures above 1000 °C provides enough time for diffusion and the formation of more inclusions, hence, lowering the corrosion resistance.
- The residual stress of AM SSs is a function of build direction, yield strength, process parameters, and shape of the part. The effect of residual stress on corrosion performance is quite complex. Compressive residual stress makes the passive film slightly denser by lowering point defect concentration. However, along with the distortion in the part, residual stress causes micro galvanic couples between regions under tensile stress and compressive stress which are the main pit initiation sites of the part.
- The surface roughness of AM parts is quite higher than other traditional manufacturing methods due to evaporation, balling phenomena, staircase effect, and facing orientation which all can be optimized by controlling the processing parameters. Decreasing the roughness of the surface diminishes the electrochemical reactions between the surface and environment leading to both general and localized corrosion reduction.
- Among alloying elements, Cr and Ni have a positive effect on the corrosion performance whether by forming the passive layer or stabilizing the austenite matrix. O is known to lower the pitting potential of AM SSs. C forms carbides and their precipitation at grain boundaries cause intergranular corrosion. The presence of Mo in the alloy composition is essential for the formation of the passive film and improves the pitting resistance. The high energy associated with the AM process causes spatially heterogeneous composition of SSs and affects the corrosion behavior based on the role of each element.
- The effect of grain size and formation of sub-structure on the corrosion performance of AM SSs is controversial in the literature. The dominant hypothesis is that super high density of sub-grain boundaries of as-fabricated SSs acts as the preferred sites for passive film nucleation resulting in a more protective surface layer. The shape of grains is important in the SCC performance of AM SSs where the elongated grains cause an anisotropic behavior against crack growth. Grain refinement processes such as heat-treatment and SPD reportedly improves the corrosion performance of stainless steels.
- AM parts produced through LPBF have almost fully austenitic microstructures by selecting proper sets of processing parameters. On the other hand, considering the slower cooling rate during the DLD method, some unwanted phases such as Intracellular δ-ferrite might be formed, which have a lower corrosion resistance compared to the austenite phase. A post-treatment might be needed to achieve a completely austenitic matrix.

Declaration of Competing Interest

The authors declare that they have no known competing financial interests or personal relationships that could have appeared to influence the work reported in this paper.

Acknowledgments

This work is supported by the NSF EPSCoR award to the state of Louisiana to establish the Consortium for Innovation in Manufacturing and Materials (CIMM), grant number NSF #OIA-1541079.

References

[1] A.J. Sedriks. Corrosion of Stainless Steel 2, 1996.
[2] M.K. Alam, M. Mehdi, R.J. Urbanic, A. Edrisy, Mechanical behavior of additive manufactured AISI 420 martensitic stainless steel, Mater. Sci. Eng. A 773 (2020), 138815.
[3] C.-O. Olsson, D. Landolt, Passive films on stainless steels—chemistry, structure and growth, Electrochim. Acta 48 (2003) 1093–1104.
[4] G. Sander, S. Thomas, V. Cruz, M. Jurg, N. Birbilis, X. Gao, M. Brameld, C. Hutchinson, On the corrosion and metastable pitting characteristics of 316L stainless steel produced by selective laser melting, J. Electrochem. Soc. 164 (2017) C250–C257.
[5] J.R. Davis, Stainless Steels, ASM international, 1994.
[6] A. Al-Amr, Mechanical Behavior and Structure of Passive Films on Austenitic Stainless Steels, 2005.
[7] L.E. Murr, E. Martinez, J. Hernandez, S. Collins, K.N. Amato, S.M. Gaytan, P. W. Shindo, Microstructures and properties of 17-4 PH stainless steel fabricated by selective laser melting, J. Mater. Res. Technol. 1 (2012) 167–177.
[8] J. Mazumder, J. Choi, K. Nagarathnam, J. Koch, D. Hetzner, The direct metal deposition of H13 tool steel for 3-D components, Jom 49 (1997) 55–60.
[9] H.D. Carlton, A. Haboub, G.F. Gallegos, D.Y. Parkinson, A.A. MacDowell, Damage evolution and failure mechanisms in additively manufactured stainless steel, Mater. Sci. Eng. A 651 (2016) 406–414.
[10] G. Casalino, S. Campanelli, N. Contuzzi, A. Ludovico, Experimental investigation and statistical optimisation of the selective laser melting process of a maraging steel, Opt. Laser Technol. 65 (2015) 151–158.
[11] T.D. Ngo, A. Kashani, G. Imbalzano, K.T. Nguyen, D. Hui, Additive manufacturing (3D printing): a review of materials, methods, applications and challenges, Compos. Part B Eng. 143 (2018) 172–196.
[12] V. Cruz, Q. Chao, N. Birbilis, D. Fabijanic, P. Hodgson, S. Thomas, Electrochemical studies on the effect of residual stress on the corrosion of 316L manufactured by selective laser melting, Corros. Sci. 164 (2020), 108314.
[13] M.A. Bevan, A. Ameri, D. East, D. Austin, A. Brown, P. Hazell, J. Escobedo-Diaz, Mechanical properties and behavior of additive manufactured stainless steel 316L. Characterization of Minerals, Metals, and Materials, Springer, 2017, pp. 577–583.
[14] W. Fredriksson, D. Petrini, K. Edström, F. Björefors, L. Nyholm, Corrosion resistances and passivation of powder metallurgical and conventionally cast 316L and 2205 stainless steels, Corros. Sci. 67 (2013) 268–280.
[15] J. Biehler, H. Hoche, M. Oechsner, P. Kaestner, K. Bunk, G. Bräuer, Influence of the microstructure on the corrosion resistance of plasma-nitrided austenitic stainless steel 304L and 316L: Einfluss des Mikrogefüges auf die Korrosionsbeständigkeit von plasmanitriertem austenitischem Stahl 1.4307 und 1.4404, Mater. Werkst. 45 (2014) 930–946.
[16] S. Washko, G. Aggen, ASM Handbook: Wrought Stainless Steels, Properties and Selection: Irons, Steels, and High-Performance Alloys, in, Ohio: ASM International, 1990.
[17] K. Geenen, A. Röttger, W. Theisen, Corrosion behavior of 316L austenitic steel processed by selective laser melting, hot-isostatic pressing, and casting, Mater. Corros. 68 (2017) 764–775.
[18] A.N. Isfahany, H. Saghafian, G. Borhani, The effect of heat treatment on mechanical properties and corrosion behavior of AISI420 martensitic stainless steel, J. Alloy. Compd. 509 (2011) 3931–3936.

[19] A. Popovich, V.S. Sufiiarov, E. Borisov, I. Polozov, D. Masaylo, A. Grigoriev, Anisotropy of mechanical properties of products manufactured using selective laser melting of powdered materials, Russ. J. Non-Ferr. Met. 58 (2017) 389–395.
[20] Y. Kok, X.P. Tan, P. Wang, M. Nai, N.H. Loh, E. Liu, S.B. Tor, Anisotropy and heterogeneity of microstructure and mechanical properties in metal additive manufacturing: a critical review, Mater. Des. 139 (2018) 565–586.
[21] J. Brnic, G. Turkalj, M. Canadija, D. Lanc, S. Krscanski, Martensitic stainless steel AISI 420—mechanical properties, creep and fracture toughness, Mech. Time-Depend. Mater. 15 (2011) 341–352.
[22] J. Hunt, F. Derguti, I. Todd, Selection of steels suitable for additive layer manufacturing, Ironmak. Steelmak. 41 (2014) 254–256.
[23] A. Yadollahi, N. Shamsaei, S.M. Thompson, A. Elwany, L. Bian, Effects of building orientation and heat treatment on fatigue behavior of selective laser melted 17-4 PH stainless steel, Int. J. Fatigue 94 (2017) 218–235.
[24] X. Lin, Y. Cao, X. Wu, H. Yang, J. Chen, W. Huang, Microstructure and mechanical properties of laser forming repaired 17-4PH stainless steel, Mater. Sci. Eng. A 553 (2012) 80–88.
[25] J.-H. Wu, C.-K. Lin, Tensile and fatigue properties of 17-4 PH stainless steel at high temperatures, Metall. Mater. Trans. A 33 (2002) 1715–1724.
[26] B.D. Craig, The effect of nickel on hydrogen cracking resistance in low alloy steels—A review, Corrosion 38 (1982) 457–463.
[27] Y. Huang, X. Yu, Q. Zhang, R. De, Marco, Corrosion performance of high strength low alloy steel AISI 4135 in the marine splash zone, Electrochemistry 85 (2017) 7–12.
[28] H. Zhang, C. Zhang, Q. Wang, C. Wu, S. Zhang, J. Chen, A.O. Abdullah, Effect of Ni content on stainless steel fabricated by laser melting deposition, Opt. Laser Technol. 101 (2018) 363–371.
[29] P. Kocovic. 3D Printing and Its Impact on the Production of Fully Functional Components: Emerging Research and Opportunities: Emerging Research and Opportunities, IGI Global, 2017.
[30] D.R. Eyers, A.T. Potter, Industrial Additive Manufacturing: a manufacturing systems perspective, Comput. Ind. 92 (2017) 208–218.
[31] C. Zeng, B. Zhang, A.H. Ettefagh, H. Wen, H. Yao, W. Meng, S. Guo, Mechanical, thermal, and corrosion properties of Cu-10Sn alloy prepared by laser-powder-bed-fusion additive manufacturing, Addit. Manuf. 35 (2020), 101411.
[32] G. Sander, J. Tan, P. Balan, O. Gharbi, D. Feenstra, L. Singer, S. Thomas, R. Kelly, J.R. Scully, N. Birbilis, Corrosion of additively manufactured alloys: a review, Corrosion 74 (2018) 1318–1350.
[33] M. Ziętala, T. Durejko, M. Polański, I. Kunce, T. Płociński, W. Zieliński, M. Łazińska, W. Stępniowski, T. Czujko, K.J. Kurzydłowski, The microstructure, mechanical properties and corrosion resistance of 316 L stainless steel fabricated using laser engineered net shaping, Mater. Sci. Eng. A 677 (2016) 1–10.
[34] C. García, F. Martín, P. De Tiedra, L.G. Cambronero, Pitting corrosion behaviour of PM austenitic stainless steels sintered in nitrogen–hydrogen atmosphere, Corros. Sci. 49 (2007) 1718–1736.
[35] J.J. Lewandowski, M. Seifi, Metal additive manufacturing: a review of mechanical properties, Annu. Rev. Mater. Res. 46 (2016) 151–186.
[36] S.M. Yusuf, N. Gao, Influence of energy density on metallurgy and properties in metal additive manufacturing, Mater. Sci. Technol. 33 (2017) 1269–1289.
[37] A.H. Ettefagh, C. Zeng, S. Guo, J. Raush, Corrosion behavior of additively manufactured Ti-6Al-4V parts and the effect of post annealing, Addit. Manuf. 28 (2019) 252–258.
[38] S.M. Yusuf, Y. Chen, S. Yang, N. Gao, Microstructural evolution and strengthening of selective laser melted 316L stainless steel processed by high-pressure torsion, Mater. Charact. 159 (2020), 110012.
[39] D. Herzog, V. Seyda, E. Wycisk, C. Emmelmann, Additive manufacturing of metals, Acta Mater. 117 (2016) 371–392.
[40] E.T. Akinlabi, R.M. Mahamood, S.A. Akinlabi, Advanced Manufacturing Techniques Using Laser Material Processing, IGI Global, 2016.
[41] S. Sun, M. Brandt, M. Easton, Powder bed fusion processes: an overview. Laser Additive Manufacturing, Elsevier, 2017, pp. 55–77.
[42] Z. Sun, X. Tan, S.B. Tor, W.Y. Yeong, Selective laser melting of stainless steel 316L with low porosity and high build rates, Mater. Des. 104 (2016) 197–204.
[43] D.D. Gu, W. Meiners, K. Wissenbach, R. Poprawe, Laser additive manufacturing of metallic components: materials, processes and mechanisms, Int. Mater. Rev. 57 (2012) 133–164.
[44] T. DebRoy, H. Wei, J. Zuback, T. Mukherjee, J. Elmer, J. Milewski, A.M. Beese, A. Wilson-Heid, A. De, W. Zhang, Additive manufacturing of metallic components–process, structure and properties, Prog. Mater. Sci. 92 (2018) 112–224.
[45] E.C. Santos, M. Shiomi, K. Osakada, T. Laoui, Rapid manufacturing of metal components by laser forming, Int. J. Mach. Tools Manuf. 46 (2006) 1459–1468.
[46] D. Kong, C. Dong, X. Ni, X. Li, Corrosion of metallic materials fabricated by selective laser melting, Npj Mater. Degrad. 3 (2019) 1–14.
[47] W. Shifeng, L. Shuai, W. Qingsong, C. Yan, Z. Sheng, S. Yusheng, Effect of molten pool boundaries on the mechanical properties of selective laser melting parts, J. Mater. Process. Technol. 214 (2014) 2660–2667.
[48] P. Ganesh, R. Giri, R. Kaul, P.R. Sankar, P. Tiwari, A. Atulkar, R. Porwal, R. Dayal, L. Kukreja, Studies on pitting corrosion and sensitization in laser rapid manufactured specimens of type 316L stainless steel, Mater. Des. 39 (2012) 509–521.
[49] D. Kong, X. Ni, C. Dong, L. Zhang, C. Man, J. Yao, K. Xiao, X. Li, Heat treatment effect on the microstructure and corrosion behavior of 316L stainless steel fabricated by selective laser melting for proton exchange membrane fuel cells, Electrochim. Acta 276 (2018) 293–303.
[50] H. Li, M. Ramezani, M. Li, C. Ma, J. Wang, Effect of process parameters on tribological performance of 316L stainless steel parts fabricated by selective laser melting, Manuf. Lett. 16 (2018) 36–39.
[51] L. Wang, S. Felicelli, Y. Gooroochurn, P. Wang, M. Horstemeyer, Optimization of the LENS® process for steady molten pool size, Mater. Sci. Eng. A 474 (2008) 148–156.
[52] R.M. Mahamood, E.T. Akinlabi, Laser additive manufacturing. 3D Printing: Breakthroughs in Research and Practice, IGI Global, 2017, pp. 154–171.
[53] C. Zhang, H. Zhang, C. Wu, S. Zhang, Z. Sun, S. Dong, Multi-layer functional graded stainless steel fabricated by laser melting deposition, Vacuum 141 (2017) 181–187.
[54] K.V. Wong, A. Hernandez, A review of additive manufacturing, Int. Sch. Res. Not. 2012 (2012).
[55] P. Ghosal, M.C. Majumder, A. Chattopadhyay, Study on direct laser metal deposition, Mater. Today Proc. 5 (2018) 12509–12518.
[56] A. Yadollahi, N. Shamsaei, S.M. Thompson, D.W. Seely, Effects of process time interval and heat treatment on the mechanical and microstructural properties of direct laser deposited 316L stainless steel, Mater. Sci. Eng. A 644 (2015) 171–183.
[57] D. Keicher, Laser engineered net shapping process. LIA Handbook of Laser Materials Processing, Laser Institute of America, Florida, 2001, pp. 561–563.
[58] E. Toyserkani, A. Khajepour, S.F. Corbin, Laser Cladding, CRC press, 2004.
[59] A. Pinkerton, W. Wang, L. Li, Component repair using laser direct metal deposition, Proc. Inst. Mech. Eng. Part B J. Eng. Manuf. 222 (2008) 827–836.
[60] M.A. Melia, H.-D.A. Nguyen, J.M. Rodelas, E.J. Schindelholz, Corrosion properties of 304L stainless steel made by directed energy deposition additive manufacturing, Corros. Sci. 152 (2019) 20–30.
[61] S.M. Yusuf, M. Nie, Y. Chen, S. Yang, N. Gao, Microstructure and corrosion performance of 316L stainless steel fabricated by selective laser melting and processed through high-pressure torsion, J. Alloy. Compd. 763 (2018) 360–375.
[62] M. Ma, Z. Wang, X. Zeng, A comparison on metallurgical behaviors of 316L stainless steel by selective laser melting and laser cladding deposition, Mater. Sci. Eng. A 685 (2017) 265–273.
[63] M. Suzuki, R. Yamaguchi, K. Murakami, M. Nakada, Inclusion particle growth during solidification of stainless steel, ISIJ Int. 41 (2001) 247–256.
[64] D. Kong, C. Dong, X. Ni, L. Zhang, C. Man, J. Yao, Y. Ji, Y. Ying, K. Xiao, X. Cheng, High-throughput fabrication of nickel-based alloys with different Nb contents via a dual-feed additive manufacturing system: effect of Nb content on microstructural and mechanical properties, J. Alloy. Compd. 785 (2019) 826–837.
[65] J. Shao, G. Yu, X. He, S. Li, R. Chen, Y. Zhao, Grain size evolution under different cooling rate in laser additive manufacturing of superalloy, Opt. Laser Technol. 119 (2019), 105662.
[66] I. Tolosa, F. Garciandía, F. Zubiri, F. Zapirain, A. Esnaola, Study of mechanical properties of AISI 316 stainless steel processed by "selective laser melting", following different manufacturing strategies, Int. J. Adv. Manuf. Technol. 51 (2010) 639–647.
[67] T. Kellner, An epiphany of disruption: GE additive chief explains how 3D printing will upend manufacturing, GE Rep. 13 (2017).
[68] P. Han, Additive design and manufacturing of jet engine parts, Engineering 3 (2017) 648–652.
[69] X. Ni, D. Kong, W. Wu, L. Zhang, C. Dong, B. He, L. Lu, K. Wu, D. Zhu, Corrosion behavior of 316L stainless steel fabricated by selective laser melting under different scanning speeds, J. Mater. Eng. Perform. 27 (2018) 3667–3677.
[70] R.F. Schaller, J.M. Taylor, J. Rodelas, E.J. Schindelholz, Corrosion properties of powder bed fusion additively manufactured 17-4 PH stainless steel, Corrosion 73 (2017) 796–807.
[71] Y. Sun, A. Moroz, K. Alrbaey, Sliding wear characteristics and corrosion behaviour of selective laser melted 316L stainless steel, J. Mater. Eng. Perform. 23 (2014) 518–526.
[72] M. Laleh, A.E. Hughes, W. Xu, P. Cizek, M.Y. Tan, Unanticipated drastic decline in pitting corrosion resistance of additively manufactured 316L stainless steel after high-temperature post-processing, Corros. Sci. 165 (2020), 108412.
[73] J.R. Trelewicz, G.P. Halada, O.K. Donaldson, G. Manogharan, Microstructure and corrosion resistance of laser additively manufactured 316L stainless steel, Jom 68 (2016) 850–859.
[74] B. Arifvianto, M. Mahardika, P. Dewo, P. Iswanto, U. Salim, Effect of surface mechanical attrition treatment (SMAT) on microhardness, surface roughness and wettability of AISI 316L, Mater. Chem. Phys. 125 (2011) 418–426.
[75] T. Roland, D. Retraint, K. Lu, J. Lu, Fatigue life improvement through surface nanostructuring of stainless steel by means of surface mechanical attrition treatment, Scr. Mater. 54 (2006) 1949–1954.
[76] C. Man, C. Dong, T. Liu, D. Kong, D. Wang, X. Li, The enhancement of microstructure on the passive and pitting behaviors of selective laser melting 316L SS in simulated body fluid, Appl. Surf. Sci. 467 (2019) 193–205.
[77] H. Hermawan, D. Ramdan, J.R. Djuansjah, Metals for biomedical applications. Biomedical Engineering-from Theory to Applications, 2011, pp. 411–430.
[78] N. Manam, W. Harun, D. Shri, S. Ghani, T. Kurniawan, M.H. Ismail, M. Ibrahim, Study of corrosion in biocompatible metals for implants: a review, J. Alloy. Compd. 701 (2017) 698–715.
[79] M. Lodhi, K. Deen, M. Greenlee-Wacker, W. Haider, Additively manufactured 316L stainless steel with improved corrosion resistance and biological response for biomedical applications, Addit. Manuf. 27 (2019) 8–19.
[80] U. Kamachimudali, T. Sridhar, B. Raj, Corrosion of bio implants, Sadhana 28 (2003) 601–637.

[81] R. Asri, W. Harun, M. Samykano, N. Lah, S. Ghani, F. Tarlochan, M. Raza, Corrosion and surface modification on biocompatible metals: a review, Mater. Sci. Eng. C 77 (2017) 1261–1274.
[82] H. Wen, C. Zeng, A. Hemmasian Ettefagh, J. Gao, S. Guo, Laser surface treatment of Ti-10Mo alloy under Ar and N2 environment for biomedical application, J. Laser Appl. 31 (2019), 022012.
[83] G. Manivasagam, D. Dhinasekaran, A. Rajamanickam, Biomedical implants: corrosion and its prevention-a review, Recent Pat. Corros. Sci. 2 (2010) 40–54.
[84] W. Harun, R. Asri, F. Romlay, S. Sharif, N. Jan, F. Tsumori, Surface characterisation and corrosion behaviour of oxide layer for SLMed-316L stainless steel, J. Alloy. Compd. 748 (2018) 1044–1052.
[85] L. Reclaru, R. Lerf, P.-Y. Eschler, J.-M. Meyer, Corrosion behavior of a welded stainless-steel orthopedic implant, Biomaterials 22 (2001) 269–279.
[86] M. Li, T. Yin, Y. Wang, F. Du, X. Zou, H. Gregersen, G. Wang, Study of biocompatibility of medical grade high nitrogen nickel-free austenitic stainless steel in vitro, Mater. Sci. Eng. C 43 (2014) 641–648.
[87] J.C. Wataha, N.L. O'Dell, B.B. Singh, M. Ghazi, G.M. Whitford, P.E. Lockwood, Relating nickel-induced tissue inflammation to nickel release in vivo, J. Biomed. Mater. Res. 58 (2001) 537–544.
[88] D. Kong, X. Ni, C. Dong, X. Lei, L. Zhang, C. Man, J. Yao, X. Cheng, X. Li, Bio-functional and anti-corrosive 3D printing 316L stainless steel fabricated by selective laser melting, Mater. Des. 152 (2018) 88–101.
[89] C.-C. Shih, C.-M. Shih, Y.-Y. Su, L.H.J. Su, M.-S. Chang, S.-J. Lin, Effect of surface oxide properties on corrosion resistance of 316L stainless steel for biomedical applications, Corros. Sci. 46 (2004) 427–441.
[90] M.P. Ryan, D.E. Williams, R.J. Chater, B.M. Hutton, D.S. McPhail, Why stainless steel corrodes, Nature 415 (2002) 770–774.
[91] D.E. Williams, M.R. Kilburn, J. Cliff, G.I. Waterhouse, Composition changes around sulphide inclusions in stainless steels, and implications for the initiation of pitting corrosion, Corros. Sci. 52 (2010) 3702–3716.
[92] I. Sailer, A. Philipp, A. Zembic, B.E. Pjetursson, C.H. Hämmerle, M. Zwahlen, A systematic review of the performance of ceramic and metal implant abutments supporting fixed implant reconstructions, Clin. Oral. Implants Res. 20 (2009) 4–31.
[93] K. Zhang, J. Zou, T. Grosdidier, C. Dong, D. Yang, Improved pitting corrosion resistance of AISI 316L stainless steel treated by high current pulsed electron beam, Surf. Coat. Technol. 201 (2006) 1393–1400.
[94] C. Carboni, P. Peyre, G. Beranger, C. Lemaitre, Influence of high power diode laser surface melting on the pitting corrosion resistance of type 316L stainless steel, J. Mater. Sci. 37 (2002) 3715–3723.
[95] A.H. Ettefagh, H. Wen, A. Chaichi, M.I. Islam, F. Lu, M. Gartia, S. Guo, Laser surface modifications of Fe-14Cr ferritic alloy for improved corrosion performance, Surf. Coat. Technol. 381 (2020), 125194.
[96] H. Yao, R. Katona, J. Zhou, M.I. Islam, J. Raush, F. Lu, S. Guo, Defects Evaluation of Selective Laser Melting Stainless Steel 316 Parts Using Positron Annihilation Lifetime Measurement, in: ASME International Mechanical Engineering Congress and Exposition, American Society of Mechanical Engineers, 2018, pp. V08BT10A057.
[97] C. Zeng, H. Wen, A.H. Ettefagh, B. Zhang, J. Gao, A. Haghshenas, J.R. Raush, S. Guo, Laser nitriding of titanium surfaces for biomedical applications, Surf. Coat. Technol. 385 (2020), 125397.
[98] J. Eric Jones, M. Chen, Q. Yu, Corrosion resistance improvement for 316L stainless steel coronary artery stents by trimethylsilane plasma nanocoatings, J. Biomed. Mater. Res. Part B Appl. Biomater. 102 (2014) 1363–1374.
[99] Y. Zhou, B. Zhang, S. Zheng, J. Wang, X. San, X. Ma, Atomic-scale decoration for improving the pitting corrosion resistance of austenitic stainless steels, Sci. Rep. 4 (2014) 3604.
[100] E. McCafferty, Effect of ion implantation on the corrosion behavior of iron, stainless steels, and aluminum—a review, Corrosion 57 (2001) 1011–1029.
[101] K. Feng, X. Cai, Z. Li, P.K. Chu, Improved corrosion resistance of stainless steel 316L by Ti ion implantation, Mater. Lett. 68 (2012) 450–452.
[102] A. Chaichi, A. Prasad, L. Kootta Parambil, S. Shaik, A. Hemmasian Ettefagh, V. Dasa, S. Guo, M.L. Osborn, R. Devireddy, M.M. Khonsari, Improvement of tribological and biocompatibility properties of orthopedic materials using piezoelectric direct discharge plasma surface modification, ACS Biomater. Sci. Eng. 5 (2019) 2147–2159.
[103] S. Anderson, Final Technical Report on Laser Direct Manufacturing (LDM) for Nuclear Power Components, DOE-NE0000542, 2015.
[104] X. Lou, M. Song, P.W. Emigh, M.A. Othon, P.L. Andresen, On the stress corrosion crack growth behaviour in high temperature water of 316L stainless steel made by laser powder bed fusion additive manufacturing, Corros. Sci. 128 (2017) 140–153.
[105] A.H. Ettefagh, H. Wen, F. Lu, S. Guo, Phase Evolution and Corrosion Performance of Laser Processed Oxide Dispersion Strengthened Ferritic Alloys, in: ASME International Mechanical Engineering Congress and Exposition, American Society of Mechanical Engineers, 2018, pp. V08BT10A058.
[106] A.S. Wu, D.W. Brown, M. Kumar, G.F. Gallegos, W.E. King, An experimental investigation into additive manufacturing-induced residual stresses in 316L stainless steel, Metall. Mater. Trans. A 45 (2014) 6260–6270.
[107] B. Verlee, T. Dormal, J. Lecomte-Beckers, Density and porosity control of sintered 316L stainless steel parts produced by additive manufacturing, Powder Metall. 55 (2012) 260–267.
[108] R.D. Hanbury, G.S. Was, Oxide growth and dissolution on 316L stainless steel during irradiation in high temperature water, Corros. Sci. 157 (2019) 305–311.
[109] X. Lou, P.L. Andresen, R.B. Rebak, Oxide inclusions in laser additive manufactured stainless steel and their effects on impact toughness and stress corrosion cracking behavior, J. Nucl. Mater. 499 (2018) 182–190.
[110] B. Stellwag, The mechanism of oxide film formation on austenitic stainless steels in high temperature water, Corros. Sci. 40 (1998) 337–370.
[111] U. Ehrnstén, Corrosion and stress corrosion cracking of austenitic stainless steels. Comprehensive Nuclear Materials, Elsevier, 2012, pp. 93–104.
[112] S.S. Raiman, D.M. Bartels, G.S. Was, Radiolysis driven changes to oxide stability during irradiation-corrosion of 316L stainless steel in high temperature water, J. Nucl. Mater. 493 (2017) 40–52.
[113] T. Terachi, T. Yamada, T. Miyamoto, K. Arioka, K. Fukuya, Corrosion behavior of stainless steels in simulated PWR primary water—effect of chromium content in alloys and dissolved hydrogen—, J. Nucl. Sci. Technol. 45 (2008) 975–984.
[114] Y. Han, J. Mei, Q. Peng, E.-H. Han, W. Ke, Effect of electropolishing on corrosion of nuclear grade 316L stainless steel in deaerated high temperature water, Corros. Sci. 112 (2016) 625–634.
[115] P. Andresen, C. Briant, Environmentally assisted cracking of types 304L/316L/316NG stainless steel in 288C water, Corrosion 45 (1989) 448–463.
[116] P. Andresen, M. Morra, Stress corrosion cracking of stainless steels and nickel alloys in high-temperature water, Corrosion 64 (2008) 15–29.
[117] P.L. Andresen, Stress corrosion cracking of current structural materials in commercial nuclear power plants, Corrosion 69 (2013) 1024–1038.
[118] G.S. Was, Y. Ashida, P.L. Andresen, Irradiation-assisted stress corrosion cracking, Corros. Rev. 29 (2011) 7–49.
[119] P.L. Andresen, M.M. Morra, IGSCC of non-sensitized stainless steels in high temperature water, J. Nucl. Mater. 383 (2008) 97–111.
[120] S.L. Hong, Influence of surface condition on primary water stress corrosion cracking initiation of alloy 600, Corrosion 57 (2001) 323–333.
[121] A. Turnbull, K. Mingard, J. Lord, B. Roebuck, D. Tice, K. Mottershead, N. Fairweather, A. Bradbury, Sensitivity of stress corrosion cracking of stainless steel to surface machining and grinding procedure, Corros. Sci. 53 (2011) 3398–3415.
[122] G. Airey, Environmental degradation of materials in nuclear power systems-water reactors, in: Proc. Int. Symp., 1983.
[123] R. Stahle, J. Hochmann, R. McCright, J. Slater, S. Shatynski, Stress corrosion cracking and hydrogen embrittlement of iron base alloys, J. Electrochem. Soc. 126 (1979) 215C, 215C-215C.
[124] D. Davies, P. Adcock, M. Turpin, S. Rowen, Stainless steel as a bipolar plate material for solid polymer fuel cells, J. Power Sources 86 (2000) 237–242.
[125] S.-J. Lee, C.-H. Huang, J.-J. Lai, Y.-P. Chen, Corrosion-resistant component for PEM fuel cells, J. Power Sources 131 (2004) 162–168.
[126] S. Karimi, N. Fraser, B. Roberts, F.R. Foulkes, A review of metallic bipolar plates for proton exchange membrane fuel cells: materials and fabrication methods, Adv. Mater. Sci. Eng. 2012 (2012) 1–22.
[127] E. Cho, U.-S. Jeon, S.-A. Hong, I.-H. Oh, S.-G. Kang, Performance of a 1 kW-class PEMFC stack using TiN-coated 316 stainless steel bipolar plates, J. Power Sources 142 (2005) 177–183.
[128] J. Wind, R. Späh, W. Kaiser, G. Böhm, Metallic bipolar plates for PEM fuel cells, J. Power Sources 105 (2002) 256–260.
[129] I. Bar-On, R. Kirchain, R. Roth, Technical cost analysis for PEM fuel cells, J. Power Sources 109 (2002) 71–75.
[130] P. Marcus, V. Maurice, H.-H. Strehblow, Localized corrosion (pitting): a model of passivity breakdown including the role of the oxide layer nanostructure, Corros. Sci. 50 (2008) 2698–2704.
[131] T.S.L. Wijesinghe, D.J. Blackwood, Real time pit initiation studies on stainless steels: the effect of sulphide inclusions, Corros. Sci. 49 (2007) 1755–1764.
[132] V. Vignal, H. Krawiec, O. Heintz, R. Oltra, The use of local electrochemical probes and surface analysis methods to study the electrochemical behaviour and pitting corrosion of stainless steels, Electrochim. Acta 52 (2007) 4994–5001.
[133] S. Okabe, M. Odagiri, T. Ito, H. Satoh, Succession of sulfur-oxidizing bacteria in the microbial community on corroding concrete in sewer systems, Appl. Environ. Microbiol. 73 (2007) 971–980.
[134] J.T. Miller, H.J. Martin, E. Cudjoe, Comparison of the effects of a sulfuric acid environment on traditionally manufactured and additive manufactured stainless steel 316L alloy, Addit. Manuf. 23 (2018) 272–286.
[135] E. Agyenim-Boateng, S. Huang, J. Sheng, G. Yuan, Z. Wang, J. Zhou, A. Feng, Influence of laser peening on the hydrogen embrittlement resistance of 316L stainless steel, Surf. Coat. Technol. 328 (2017) 44–53.
[136] J. He, G. Han, S. Fukuyama, K. Yokogawa, A. Kimura, Effect of hydrogen on dynamic precipitation of carbide in type 304 stainless steel during creep process, Acta Mater. 45 (1997) 3377–3388.
[137] R. Silverstein, D. Eliezer, Hydrogen trapping in 3D-printed (additive manufactured) Ti-6Al-4V, Mater. Charact. 144 (2018) 297–304.
[138] D. Itzhak, E. Aghion, Corrosion behaviour of hot-pressed austenitic stainless steel in H2SO4 solutions at room temperature, Corros. Sci. 23 (1983) 1085–1094.
[139] E. Otero, A. Pardo, M. Utrilla, E. Sáenz, F. Perez, Influence of microstructure on the corrosion resistance of AISI type 304L and type 316L sintered stainless steels exposed to ferric chloride solution, Mater. Charact. 35 (1995) 145–151.
[140] E. Otero, A. Pardo, M. Utrilla, E. Saenz, J. Alvarez, Corrosion behaviour of AISI 304L and 316L stainless steels prepared by powder metallurgy in the presence of sulphuric and phosphoric acid, Corros. Sci. 40 (1998) 1421–1434.
[141] Q. Meng, G. Frankel, H. Colijn, S. Goss, Stainless-steel corrosion and MnS inclusions, Nature 424 (2003) 389–390.
[142] M. Lodhi, K. Deen, W. Haider, Corrosion behavior of additively manufactured 316L stainless steel in acidic media, Materialia 2 (2018) 111–121.

[143] S.V. Muley, A.N. Vidvans, G.P. Chaudhari, S. Udainiya, An assessment of ultra fine grained 316L stainless steel for implant applications, Acta Biomater. 30 (2016) 408–419.
[144] M. Pisarek, P. Kędzierzawski, M. Janik-Czachor, K. Kurzydłowski, The effect of hydrostatic extrusion on resistance of 316 austenitic stainless steel to pit nucleation, Electrochem. Commun. 9 (2007) 2463–2466.
[145] Z. Zheng, Y. Gao, Y. Gui, M. Zhu, Corrosion behaviour of nanocrystalline 304 stainless steel prepared by equal channel angular pressing, Corros. Sci. 54 (2012) 60–67.
[146] T. Massoud, V. Maurice, L.H. Klein, P. Marcus, Nanoscale morphology and atomic structure of passive films on stainless steel, J. Electrochem. Soc. 160 (2013) C232–C238.
[147] V. Vignal, H. Krawiec, O. Heintz, D. Mainy, Passive properties of lean duplex stainless steels after long-term ageing in air studied using EBSD, AES, XPS and local electrochemical impedance spectroscopy, Corros. Sci. 67 (2013) 109–117.
[148] C.Q. Cheng, J. Zhao, T.S. Cao, Q.Q. Fu, M.K. Lei, Facile chromaticity approach for the inspection of passive films on austenitic stainless steel, Corros. Sci. 70 (2013) 235–242.
[149] G. Lorang, M.D.C. Belo, A. Simoes, M. Ferreira, Chemical composition of passive films on AISI 304 stainless steel, J. Electrochem. Soc. 141 (1994) 3347–3356.
[150] L. Freire, M. Carmezim, Ma Ferreira, M. Montemor, The passive behaviour of AISI 316 in alkaline media and the effect of pH: a combined electrochemical and analytical study, Electrochim. Acta 55 (2010) 6174–6181.
[151] M. Carmezim, A. Simoes, M. Montemor, M.D.C. Belo, Capacitance behaviour of passive films on ferritic and austenitic stainless steel, Corros. Sci. 47 (2005) 581–591.
[152] A. Fattah-Alhosseini, M. Golozar, A. Saatchi, K. Raeissi, Effect of solution concentration on semiconducting properties of passive films formed on austenitic stainless steels, Corros. Sci. 52 (2010) 205–209.
[153] K. Habib, M. Damra, J. Saura, I. Cervera, J. Bellés, Breakdown and evolution of the protective oxide scales of AISI 304 and AISI 316 stainless steels under high-temperature oxidation, Int. J. Corros. 2011 (2011) 1–10.
[154] M. Sun, X. Wu, Z. Zhang, E.-H. Han, Oxidation of 316 stainless steel in supercritical water, Corros. Sci. 51 (2009) 1069–1072.
[155] J. Stewart, D. Williams, The initiation of pitting corrosion on austenitic stainless steel: on the role and importance of sulphide inclusions, Corros. Sci. 33 (1992) 457–474.
[156] B. Lu, J. Luo, F. Mohammadi, K. Wang, X. Wan, Correlation between repassivation kinetics and corrosion rate over a passive surface in flowing slurry, Electrochim. Acta 53 (2008) 7022–7031.
[157] D. Kong, C. Dong, X. Ni, L. Zhang, J. Yao, C. Man, X. Cheng, K. Xiao, X. Li, Mechanical properties and corrosion behavior of selective laser melted 316L stainless steel after different heat treatment processes, J. Mater. Sci. Technol. 35 (2019) 1499–1507.
[158] J. Čapek, M. Machová, M. Fousová, J. Kubásek, D. Vojtěch, J. Fojt, E. Jablonska, J. Lipov, T. Ruml, Highly porous, low elastic modulus 316L stainless steel scaffold prepared by selective laser melting, Mater. Sci. Eng. C 69 (2016) 631–639.
[159] G. Burstein, C. Liu, R. Souto, S. Vines, Origins of pitting corrosion, Corros. Eng. Sci. Technol. 39 (2004) 25–30.
[160] M. Laleh, A.E. Hughes, W. Xu, I. Gibson, M.Y. Tan, Unexpected erosion-corrosion behaviour of 316L stainless steel produced by selective laser melting, Corros. Sci. 155 (2019) 67–74.
[161] W. Harun, R. Asri, J. Alias, F. Zulkifli, K. Kadirgama, S. Ghani, J. Shariffuddin, A comprehensive review of hydroxyapatite-based coatings adhesion on metallic biomaterials, Ceram. Int. 44 (2018) 1250–1268.
[162] S. Kumar, T.S. Narayanan, S.G.S. Raman, S. Seshadri, Thermal oxidation of CP-Ti: evaluation of characteristics and corrosion resistance as a function of treatment time, Mater. Sci. Eng. C 29 (2009) 1942–1949.
[163] M.Z. Ibrahim, A.A. Sarhan, F. Yusuf, M. Hamdi, Biomedical materials and techniques to improve the tribological, mechanical and biomedical properties of orthopedic implants–A review article, J. Alloy. Compd. 714 (2017) 636–667.
[164] H. Buscail, S. El Messki, F. Riffard, S. Perrier, R. Cueff, E. Caudron, C. Issartel, Characterization of the oxides formed at 1000°C on the AISI 316L stainless steel—Role of molybdenum, Mater. Chem. Phys. 111 (2008) 491–496.
[165] S. Zhang, R. Shi, Y. Chen, M. Wang, Corrosion behavior of oxide films on AISI 316L SS formed in high temperature water with simultaneous injection of zinc and aluminum, J. Alloy. Compd. 731 (2018) 1230–1237.
[166] D. Herzog, V. Seyda, E. Wycisk, C. Emmelmann, Additive manufacturing of metals, Acta Mater. 117 (2016) 371–392.
[167] W.J. Sames, F. List, S. Pannala, R.R. Dehoff, S.S. Babu, The metallurgy and processing science of metal additive manufacturing, Int. Mater. Rev. 61 (2016) 315–360.
[168] G. Miranda, S. Faria, F. Bartolomeu, E. Pinto, S. Madeira, A. Mateus, P. Carreira, N. Alves, F. Silva, O. Carvalho, Predictive models for physical and mechanical properties of 316L stainless steel produced by selective laser melting, Mater. Sci. Eng. A 657 (2016) 43–56.
[169] M.S.F. de Lima, S. Sankaré, Microstructure and mechanical behavior of laser additive manufactured AISI 316 stainless steel stringers, Mater. Des. 55 (2014) 526–532.
[170] S. Kavousi, B.R. Novak, J. Hoyt, D. Moldovan, Interface kinetics of rapid solidification of binary alloys by atomistic simulations: application to Ti-Ni alloys, Comput. Mater. Sci. 184 (2020), 109854.
[171] D. Gu, Y. Shen, Balling phenomena in direct laser sintering of stainless steel powder: metallurgical mechanisms and control methods, Mater. Des. 30 (2009) 2903–2910.
[172] J.-P. Kruth, L. Froyen, J. Van Vaerenbergh, P. Mercelis, M. Rombouts, B. Lauwers, Selective laser melting of iron-based powder, J. Mater. Process. Technol. 149 (2004) 616–622.
[173] S. Gorsse, C. Hutchinson, M. Gouné, R. Banerjee, Additive manufacturing of metals: a brief review of the characteristic microstructures and properties of steels, Ti-6Al-4V and high-entropy alloys, Sci. Technol. Adv. Mater. 18 (2017) 584–610.
[174] C. Barile, C. Casavola, S. Campanelli, G. Renna, Analysis of corrosion on sintered stainless steel: mechanical and physical aspects, Eng. Fail. Anal. 95 (2019) 273–282.
[175] N. Dai, J. Zhang, Y. Chen, L.-C. Zhang, Heat treatment degrading the corrosion resistance of selective laser melted Ti-6Al-4V alloy, J. Electrochem. Soc. 164 (2017) C428–C434.
[176] J. Suryawanshi, K. Prashanth, U. Ramamurty, Mechanical behavior of selective laser melted 316L stainless steel, Mater. Sci. Eng. A 696 (2017) 113–121.
[177] M. Laleh, A.E. Hughes, S. Yang, J. Li, W. Xu, I. Gibson, M.Y. Tan, Two and three-dimensional characterisation of localised corrosion affected by lack-of-fusion pores in 316L stainless steel produced by selective laser melting, Corros. Sci. 165 (2020), 108394.
[178] M. Rahimi, S. Tabaian, S. Marashi, S. Saramad, M. Arab, A. Hemasian, Heat treatment of aluminum in preparing porous anodic alumina templates, Micro Nano Lett. 7 (2012) 125–129..
[179] A.L. Maximenko, E.A. Olevsky, Pore filling during selective laser melting-assisted additive manufacturing of composites, Scr. Mater. 149 (2018) 75–78.
[180] R. Laquai, B.R. Müller, G. Kasperovich, J. Haubrich, G. Requena, G. Bruno, X-ray refraction distinguishes unprocessed powder from empty pores in selective laser melting Ti-6Al-4V, Mater. Res. Lett. 6 (2018) 130–135.
[181] R.F. Schaller, A. Mishra, J.M. Rodelas, J.M. Taylor, E.J. Schindelholz, The role of microstructure and surface finish on the corrosion of selective laser melted 304L, J. Electrochem. Soc. 165 (2018) C234–C242.
[182] J. Suryawanshi, T. Baskaran, O. Prakash, S. Arya, U. Ramamurty, On the corrosion resistance of some selective laser melted alloys, Materialia 3 (2018) 153–161.
[183] C. Prieto, M. Singer, T. Cyders, D. Young, Investigation of pitting corrosion initiation and propagation of a type 316L stainless steel manufactured by the direct metal laser sintering process, Corrosion 75 (2019) 140–143.
[184] S. Wolff, T. Lee, E. Faierson, K. Ehmann, J. Cao, Anisotropic properties of directed energy deposition (DED)-processed Ti–6Al–4V, J. Manuf. Process. 24 (2016) 397–405.
[185] C. Zhou, S. Hu, Q. Shi, H. Tao, Y. Song, J. Zheng, P. Xu, L. Zhang, Improvement of corrosion resistance of SS316L manufactured by selective laser melting through subcritical annealing, Corros. Sci. 164 (2020), 108353.
[186] Y. Zhang, F. Liu, J. Chen, Y. Yuan, Effects of surface quality on corrosion resistance of 316L stainless steel parts manufactured via SLM, J. Laser Appl. 29 (2017), 022306.
[187] Q. Chao, V. Cruz, S. Thomas, N. Birbilis, P. Collins, A. Taylor, P.D. Hodgson, D. Fabijanic, On the enhanced corrosion resistance of a selective laser melted austenitic stainless steel, Scr. Mater. 141 (2017) 94–98.
[188] P. Pistorius, G. Burstein, Metastable pitting corrosion of stainless steel and the transition to stability, Philos. Trans. R. Soc. Lond. Ser. A Phys. Eng. Sci. 341 (1992) 531–559.
[189] A.T. Sutton, C.S. Kriewall, M.C. Leu, J.W. Newkirk, Powder characterisation techniques and effects of powder characteristics on part properties in powder-bed fusion processes, Virtual Phys. Prototyp. 12 (2017) 3–29.
[190] R. Li, Y. Shi, Z. Wang, L. Wang, J. Liu, W. Jiang, Densification behavior of gas and water atomized 316L stainless steel powder during selective laser melting, Appl. Surf. Sci. 256 (2010) 4350–4356.
[191] J. Kluczyński, L. Śnieżek, K. Grzelak, J. Mierzyński, The influence of exposure energy density on porosity and microhardness of the SLM additive manufactured elements, Materials 11 (2018) 2304.
[192] I. Maskery, N. Aboulkhair, M. Corfield, C. Tuck, A. Clare, R.K. Leach, R. D. Wildman, I. Ashcroft, R.J. Hague, Quantification and characterisation of porosity in selectively laser melted Al–Si10–Mg using X-ray computed tomography, Mater. Charact. 111 (2016) 193–204.
[193] T. Vilaro, C. Colin, J.-D. Bartout, As-fabricated and heat-treated microstructures of the Ti-6Al-4V alloy processed by selective laser melting, Metall. Mater. Trans. A 42 (2011) 3190–3199.
[194] J. Cherry, H. Davies, S. Mehmood, N. Lavery, S. Brown, J. Sienz, Investigation into the effect of process parameters on microstructural and physical properties of 316L stainless steel parts by selective laser melting, Int. J. Adv. Manuf. Technol. 76 (2015) 869–879.
[195] S.M. Yusuf, Y. Chen, R. Boardman, S. Yang, N. Gao, Investigation on porosity and microhardness of 316L stainless steel fabricated by selective laser melting, Metals 7 (2017) 64.
[196] A.H. Ettefagh, S. Guo, Electrochemical behavior of AISI316L stainless steel parts produced by laser-based powder bed fusion process and the effect of post annealing process, Addit. Manuf. 22 (2018) 153–156.
[197] M. Baker, J. Castle, The initiation of pitting corrosion at MnS inclusions, Corros. Sci. 34 (1993) 667–682.
[198] J. Jun, K. Holguin, G. Frankel, Pitting corrosion of very clean type 304 stainless steel, Corrosion 70 (2014) 146–155.
[199] R. Lillard, M. Kashfipour, W. Niu, Pit propagation at the boundary between manganese sulfide inclusions and austenitic stainless steel 303 and the role of copper, J. Electrochem. Soc. 163 (2016) C440–C451.
[200] A. Hemmasian-Ettefagh, M. Amiri, C. Dehghanian, Corrosion inhibition of carbon steel in cooling water, Mater. Perform. 49 (2010) 60–65.

[201] R. Reed, Materials at Low Temperatures, 154, American Society for Metals, Metals Park, Ohio, 1983.
[202] J. Castle, R. Ke, Studies by auger spectroscopy of pit initiation at the site of inclusions in stainless steel, Corros. Sci. 30 (1990) 409–428.
[203] R. Ke, R. Alkire, Initiation of corrosion pits at inclusions on 304 stainless steel, J. Electrochem. Soc. 142 (1995) 4056–4062.
[204] A. Chiba, I. Muto, Y. Sugawara, N. Hara, Pit initiation mechanism at MnS inclusions in stainless steel: synergistic effect of elemental sulfur and chloride ions, J. Electrochem. Soc. 160 (2013) C511–C520.
[205] H. Krawiec, V. Vignal, O. Heintz, R. Oltra, J.-M. Olive, Influence of the chemical dissolution of MnS inclusions on the electrochemical behavior of stainless steels, J. Electrochem. Soc. 152 (2005) B213.
[206] G. Sander, S. Thomas, V. Cruz, M. Jurg, N. Birbilis, X. Gao, M. Brameld, C. Hutchinson, On the corrosion and metastable pitting characteristics of 316L stainless steel produced by selective laser melting, J. Electrochem. Soc. 164 (2017) C250–C257.
[207] K. Saeidi, X. Gao, Y. Zhong, Z.J. Shen, Hardened austenite steel with columnar sub-grain structure formed by laser melting, Mater. Sci. Eng. A 625 (2015) 221–229.
[208] T. Kurzynowski, K. Gruber, W. Stopyra, B. Kuźnicka, E. Chlebus, Correlation between process parameters, microstructure and properties of 316 L stainless steel processed by selective laser melting, Mater. Sci. Eng. A 718 (2018) 64–73.
[209] S. Zheng, C. Li, Y. Qi, L. Chen, C. Chen, Mechanism of (Mg, Al, Ca)-oxide inclusion-induced pitting corrosion in 316L stainless steel exposed to sulphur environments containing chloride ion, Corros. Sci. 67 (2013) 20–31.
[210] C. Man, Z. Duan, Z. Cui, C. Dong, D. Kong, T. Liu, S. Chen, X. Wang, The effect of sub-grain structure on intergranular corrosion of 316L stainless steel fabricated via selective laser melting, Mater. Lett. 243 (2019) 157–160.
[211] D. Kong, C. Dong, Z. Zheng, F. Mao, A. Xu, X. Ni, C. Man, J. Yao, K. Xiao, X. Li, Surface monitoring for pitting evolution into uniform corrosion on Cu-Ni-Zn ternary alloy in alkaline chloride solution: ex-situ LCM and in-situ SECM, Appl. Surf. Sci. 440 (2018) 245–257.
[212] M. Shiomi, K. Osakada, K. Nakamura, T. Yamashita, F. Abe, Residual stress within metallic model made by selective laser melting process, CIRP Ann. 53 (2004) 195–198.
[213] P. Mercelis, J.P. Kruth, Residual stresses in selective laser sintering and selective laser melting, Rapid Prototyp. J. 12 (2006) 254–265.
[214] G.S. Schajer, Practical Residual Stress Measurement Methods, John Wiley & Sons, 2013.
[215] I. Yadroitsev, I. Yadroitsava, Evaluation of residual stress in stainless steel 316L and Ti6Al4V samples produced by selective laser melting, Virtual Phys. Prototyp. 10 (2015) 67–76.
[216] C. Li, Z. Liu, X. Fang, Y. Guo, Residual stress in metal additive manufacturing, Procedia CIRP 71 (2018) 348–353.
[217] X. Zhao, A. Iyer, P. Promoppatum, S.-C. Yao, Numerical modeling of the thermal behavior and residual stress in the direct metal laser sintering process of titanium alloy products, Addit. Manuf. 14 (2017) 126–136.
[218] J.L. Bartlett, X. Li, An overview of residual stresses in metal powder bed fusion, Addit. Manuf. 27 (2019) 131–149.
[219] P.J. Withers, H. Bhadeshia, Residual stress. Part 1–measurement techniques, Mater. Sci. Technol. 17 (2001) 355–365.
[220] D. Tomus, Y. Tian, P.A. Rometsch, M. Heilmaier, X. Wu, Influence of post heat treatments on anisotropy of mechanical behaviour and microstructure of Hastelloy-X parts produced by selective laser melting, Mater. Sci. Eng. A 667 (2016) 42–53.
[221] C. Li, R. White, X. Fang, M. Weaver, Y. Guo, Microstructure evolution characteristics of Inconel 625 alloy from selective laser melting to heat treatment, Mater. Sci. Eng. A 705 (2017) 20–31.
[222] C. Barile, C. Casavola, G. Pappalettera, C. Pappalettere, Overview of the effects of process parameters on the accuracy in residual stress measurements by using HD and ESPI. Residual Stress, Thermomechanics & Infrared Imaging, Hybrid Techniques and Inverse Problems Volume 9, Springer, 2016, pp. 113–118.
[223] V. Hauk, 2-x-ray diffraction, Structural and Residual Stress Analysis by Nondestructive Methods, Elsevier Science BV, Amsterdam, 1997, p. 17.
[224] Q. Luo, A. Jones, High-precision determination of residual stress of polycrystalline coatings using optimised XRD-sin2ψ technique, Surf. Coat. Technol. 205 (2010) 1403–1408.
[225] T. Mukherjee, W. Zhang, T. DebRoy, An improved prediction of residual stresses and distortion in additive manufacturing, Comput. Mater. Sci. 126 (2017) 360–372.
[226] F. Navai, Effects of tensile and compressive stresses on the passive layers formed on a type 302 stainless steel in a normal sulphuric acid bath, J. Mater. Sci. 30 (1995) 1166–1172.
[227] O. Takakuwa, H. Soyama, Effect of residual stress on the corrosion behavior of austenitic stainless steel, Adv. Chem. Eng. Sci. 5 (2014) 62–71.
[228] P. Peyre, C. Carboni, P. Forget, G. Beranger, C. Lemaitre, D. Stuart, Influence of thermal and mechanical surface modifications induced by laser shock processing on the initiation of corrosion pits in 316L stainless steel, J. Mater. Sci. 42 (2007) 6866–6877.
[229] P. Peyre, X. Scherpereel, L. Berthe, C. Carboni, R. Fabbro, G. Béranger, C. Lemaitre, Surface modifications induced in 316L steel by laser peening and shot-peening. Influence on pitting corrosion resistance, Mater. Sci. Eng. A 280 (2000) 294–302.
[230] T. Simson, A. Emmel, A. Dwars, J. Böhm, Residual stress measurements on AISI 316L samples manufactured by selective laser melting, Addit. Manuf. 17 (2017) 183–189.
[231] C. Örnek, S.A. Idris, P. Reccagni, D.L. Engelberg, Atmospheric-induced stress corrosion cracking of grade 2205 duplex stainless steel—effects of 475C embrittlement and process orientation, Metals 6 (2016) 167.
[232] F. Almuaili, S. McDonald, P. Withers, A. Cook, D. Engelberg, Strain-induced reactivation of corrosion pits in austenitic stainless steel, Corros. Sci. 125 (2017) 12–19.
[233] C. Örnek, D. Engelberg, Towards understanding the effect of deformation mode on stress corrosion cracking susceptibility of grade 2205 duplex stainless steel, Mater. Sci. Eng. A 666 (2016) 269–279.
[234] A.P. Jirandehi, M. Mehdizadeh, M. Khonsari, Temperature-induced buckling of ductile metals during cyclic loading and the subsequent early fracture, Int. J. Mech. Sci. 176 (2020), 105525.
[235] G. Van Boven, W. Chen, R. Rogge, The role of residual stress in neutral pH stress corrosion cracking of pipeline steels. Part I: Pitting and cracking occurrence, Acta Mater. 55 (2007) 29–42.
[236] W. Chen, G. Van Boven, R. Rogge, The role of residual stress in neutral pH stress corrosion cracking of pipeline steels–Part II: crack dormancy, Acta Mater. 55 (2007) 43–53.
[237] C. Örnek, Additive manufacturing–a general corrosion perspective, Corros. Eng. Sci. Technol. 53 (2018) 531–535.
[238] D. Buchbinder, W. Meiners, N. Pirch, K. Wissenbach, J. Schrage, Investigation on reducing distortion by preheating during manufacture of aluminum components using selective laser melting, J. Laser Appl. 26 (2014), 012004.
[239] M.F. Zaeh, G. Branner, Investigations on residual stresses and deformations in selective laser melting, Prod. Eng. 4 (2010) 35–45.
[240] J.-P. Kruth, J. Deckers, E. Yasa, R. Wauthlé, Assessing and comparing influencing factors of residual stresses in selective laser melting using a novel analysis method, Proc. Inst. Mech. Eng. Part B J. Eng. Manuf. 226 (2012) 980–991.
[241] M. Montero Sistiaga, S. Nardone, C. Hautfenne, J. Van Humbeeck, Effect of heat treatment of 316L stainless steel produced by selective laser melting (SLM), in: Proceedings of the 27th Annual International Solid Freeform Fabrication Symposium-An Additive Manufacturing Conference, 2016, pp. 558–565.
[242] Y. Zuo, H. Wang, J. Xiong, The aspect ratio of surface grooves and metastable pitting of stainless steel, Corros. Sci. 44 (2002) 25–35.
[243] A. Shahryari, W. Kamal, S. Omanovic, The effect of surface roughness on the efficiency of the cyclic potentiodynamic passivation (CPP) method in the improvement of general and pitting corrosion resistance of 316LVM stainless steel, Mater. Lett. 62 (2008) 3906–3909.
[244] D. Wang, Y. Liu, Y. Yang, D. Xiao, Theoretical and experimental study on surface roughness of 316L stainless steel metal parts obtained through selective laser melting, Rapid Prototyp. J. 22 (2016) 706–716.
[245] J.C. Fox, S.P. Moylan, B.M. Lane, Effect of process parameters on the surface roughness of overhanging structures in laser powder bed fusion additive manufacturing, Procedia CIRP 45 (2016) 131–134.
[246] M. Jamshidinia, R. Kovacevic, The influence of heat accumulation on the surface roughness in powder-bed additive manufacturing, Surf. Topogr. Metrol. Prop. 3 (2015), 014003.
[247] J. Gockel, L. Sheridan, B. Koerper, B. Whip, The influence of additive manufacturing processing parameters on surface roughness and fatigue life, Int. J. Fatigue 124 (2019) 380–388.
[248] Y. Tian, D. Tomus, P. Rometsch, X. Wu, Influences of processing parameters on surface roughness of Hastelloy X produced by selective laser melting, Addit. Manuf. 13 (2017) 103–112.
[249] H. Chen, D. Gu, J. Xiong, M. Xia, Improving additive manufacturing processability of hard-to-process overhanging structure by selective laser melting, J. Mater. Process. Technol. 250 (2017) 99–108.
[250] G. Strano, L. Hao, R.M. Everson, K.E. Evans, Surface roughness analysis, modelling and prediction in selective laser melting, J. Mater. Process. Technol. 213 (2013) 589–597.
[251] C. Qiu, C. Panwisawas, M. Ward, H.C. Basoalto, J.W. Brooks, M.M. Attallah, On the role of melt flow into the surface structure and porosity development during selective laser melting, Acta Mater. 96 (2015) 72–79.
[252] D.N. Aqilah, Y. Farazila, D.Y. Suleiman, M.A.N. Amirah, W.B.W.N. Izzati, Effects of process parameters on the surface roughness of stainless steel 316L parts produced by selective laser melting, J. Test. Eval. 46 (2018) 1673–1683.
[253] N.T. Aboulkhair, I. Maskery, C. Tuck, I. Ashcroft, N.M. Everitt, On the formation of AlSi10Mg single tracks and layers in selective laser melting: microstructure and nano-mechanical properties, J. Mater. Process. Technol. 230 (2016) 88–98.
[254] F. Calignano, D. Manfredi, E. Ambrosio, L. Iuliano, P. Fino, Influence of process parameters on surface roughness of aluminum parts produced by DMLS, Int. J. Adv. Manuf. Technol. 67 (2013) 2743–2751.
[255] I. Yadroitsev, P. Bertrand, I. Smurov, Parametric analysis of the selective laser melting process, Appl. Surf. Sci. 253 (2007) 8064–8069.
[256] I. Yadroitsev, L. Thivillon, P. Bertrand, I. Smurov, Strategy of manufacturing components with designed internal structure by selective laser melting of metallic powder, Appl. Surf. Sci. 254 (2007) 980–983.
[257] P. Thomsen, J. Malmström, L. Emanuelsson, M. Rene, A. Snis, Electron beam-melted, free-form-fabricated titanium alloy implants: material surface characterization and early bone response in rabbits, J. Biomed. Mater. Res. Part B Appl. Biomater. 90 (2009) 35–44.
[258] A. Barari, H. Kishawy, F. Kaji, M. Elbestawi, On the surface quality of additive manufactured parts, Int. J. Adv. Manuf. Technol. 89 (2017) 1969–1974.
[259] A. Triantaphyllou, C.L. Giusca, G.D. Macaulay, F. Roerig, M. Hoebel, R.K. Leach, B. Tomita, K.A. Milne, Surface texture measurement for additive manufacturing, Surf. Topogr. Metrol. Prop. 3 (2015), 024002.

[260] P. Bacchewar, S. Singhal, P. Pandey, Statistical modelling and optimization of surface roughness in the selective laser sintering process, Proc. Inst. Mech. Eng. Part B J. Eng. Manuf. 221 (2007) 35–52.
[261] L. Gil, S. Brühl, L. Jiménez, O. Leon, R. Guevara, M.H. Staia, Corrosion performance of the plasma nitrided 316L stainless steel, Surf. Coat. Technol. 201 (2006) 4424–4429.
[262] H. Abedi, M. Salehi, M. Yazdkhasti, A. Hemmasian-E, Effect of high temperature post-oxidizing on tribological and corrosion behavior of plasma nitrided AISI 316 austenitic stainless steel, Vacuum 85 (2010) 443–447.
[263] K. Yang, Y. Ren, Nickel-free austenitic stainless steels for medical applications, Sci. Technol. Adv. Mater. 11 (2010), 014105.
[264] V. Gavriljuk, B. Shanina, H. Berns, On the correlation between electron structure and short range atomic order in iron-based alloys, Acta Mater. 48 (2000) 3879–3893.
[265] P. Levey, A. Van Bennekom, A mechanistic study of the effects of nitrogen on the corrosion properties of stainless steels, Corrosion 51 (1995) 911–921.
[266] H. Baba, T. Kodama, Y. Katada, Role of nitrogen on the corrosion behavior of austenitic stainless steels, Corros. Sci. 44 (2002) 2393–2407.
[267] R. Jargelius-Pettersson, Electrochemical investigation of the influence of nitrogen alloying on pitting corrosion of austenitic stainless steels, Corros. Sci. 41 (1999) 1639–1664.
[268] H. Feichtinger, G. Stein, Melting of high nitrogen steels. Materials Science Forum, Trans Tech Publ, 1999, pp. 261–270.
[269] M. Pridantsev, F. Levin, Effect of manganese on the structure and properties of nonmagnetic stainless steels, Met. Sci. Heat Treat. 7 (1966) 786–789.
[270] C. Cui, V. Uhlenwinkel, A. Schulz, H.-W. Zoch, Austenitic stainless steel powders with increased nitrogen content for laser additive manufacturing, Metals 10 (2020) 61.
[271] J. Gubicza, M. El-Tahawy, Y. Huang, H. Choi, H. Choe, J.L. Lábár, T.G. Langdon, Microstructure, phase composition and hardness evolution in 316L stainless steel processed by high-pressure torsion, Mater. Sci. Eng. A 657 (2016) 215–223.
[272] C.R. Clayton, G.P. Halada, J.R. Kearns, Passivity of high-nitrogen stainless alloys: the role of metal oxyanions and salt films, Mater. Sci. Eng. 198 (1995) 135–144.
[273] G. Halada, C. Clayton, Comparison of Mo–N and W–N synergism during passivation of stainless steel through x-ray photoelectron spectroscopy and electrochemical analysis, J. Vac. Sci. Technol. A Vac. Surf. Films 11 (1993) 2342–2347.
[274] M. Yakout, A. Cadamuro, M. Elbestawi, S.C. Veldhuis, The selection of process parameters in additive manufacturing for aerospace alloys, Int. J. Adv. Manuf. Technol. 92 (2017) 2081–2098.
[275] X. He, T. DebRoy, P. Fuerschbach, Alloying element vaporization during laser spot welding of stainless steel, J. Phys. D Appl. Phys. 36 (2003) 3079–3088.
[276] M. Yakout, M. Elbestawi, S.C. Veldhuis, On the characterization of stainless steel 316L parts produced by selective laser melting, Int. J. Adv. Manuf. Technol. 95 (2018) 1953–1974.
[277] A. Di Schino, J. Kenny, Effects of the grain size on the corrosion behavior of refined AISI 304 austenitic stainless steels, J. Mater. Sci. Lett. 21 (2002) 1631–1634.
[278] Y. Li, F. Wang, G. Liu, Grain size effect on the electrochemical corrosion behavior of surface nanocrystallized low-carbon steel, Corrosion 60 (2004) 891–896.
[279] Y.-w Hao, B. Deng, C. Zhong, Y.-m Jiang, J. Li, Effect of surface mechanical attrition treatment on corrosion behavior of 316 stainless steel, J. Iron Steel Res. Int. 16 (2009) 68–72.
[280] J. Lei, J. Xie, S. Zhou, H. Song, X. Song, X. Zhou, Comparative study on microstructure and corrosion performance of 316 stainless steel prepared by laser melting deposition with ring-shaped beam and Gaussian beam, Opt. Laser Technol. 111 (2019) 271–283.
[281] X.-q Ni, D.-c Kong, Y. Wen, L. Zhang, W.-h Wu, B.-b He, L. Lu, D.-x Zhu, Anisotropy in mechanical properties and corrosion resistance of 316L stainless steel fabricated by selective laser melting, Int. J. Miner. Metall. Mater. 26 (2019) 319–328.
[282] H.H. Alsalla, C. Smith, L. Hao, Effect of build orientation on the surface quality, microstructure and mechanical properties of selective laser melting 316L stainless steel, Rapid Prototyp. J. 24 (2018) 9–17.
[283] C. Kamath, B. El-Dasher, G.F. Gallegos, W.E. King, A. Sisto, Density of additively-manufactured, 316L SS parts using laser powder-bed fusion at powers up to 400 W, Int. J. Adv. Manuf. Technol. 74 (2014) 65–78.
[284] D. Kong, C. Dong, X. Ni, L. Zhang, H. Luo, R. Li, L. Wang, C. Man, X. Li, The passivity of selective laser melted 316L stainless steel, Appl. Surf. Sci. 504 (2020), 144495.
[285] G. Wang, Q. Liu, H. Rao, H. Liu, C. Qiu, Influence of porosity and microstructure on mechanical and corrosion properties of a selectively laser melted stainless steel, J. Alloy. Compd. 831 (2020), 154815.
[286] A. Strondl, O. Lyckfeldt, H. Brodin, U. Ackelid, Characterization and control of powder properties for additive manufacturing, Jom 67 (2015) 549–554.
[287] M. Galati, L. Iuliano, A. Salmi, E. Atzeni, Modelling energy source and powder properties for the development of a thermal FE model of the EBM additive manufacturing process, Addit. Manuf. 14 (2017) 49–59.
[288] E.H. Valente, T.L. Christiansen, M.A. Somers, The Effect of Heat Treatment and Surface Hardening of 3D Printed Austenitic Stainless Steel AISI316l on Corrosion and Wear Properties, in: ESSC & DUPLEX 2019, 2019.
[289] A.P. Jirandehi, T. Chakherlou, A fatigue crack initiation and growth life estimation method in single-bolted connections, J. Strain Anal. Eng. Des. 54 (2019) 79–94.
[290] B. Zhang, M. Dodaran, S. Ahmed, S. Shao, W. Meng, K. Juul, K. Nielsen, Grain-size affected mechanical response and deformation behavior in microscale reverse extrusion, Materialia 6 (2019), 100272.
[291] C.C. Mohan, A. Prabhath, A.M. Cherian, S. Vadukumpully, S.V. Nair, K. Chennazhi, D. Menon, Nanotextured stainless steel for improved corrosion resistance and biological response in coronary stenting, Nanoscale 7 (2015) 832–841.
[292] X. Zhang, M. Shi, C. Li, N. Liu, Y. Wei, The influence of grain size on the corrosion resistance of nanocrystalline zirconium metal, Mater. Sci. Eng. A 448 (2007) 259–263.
[293] R. Misra, C. Nune, T. Pesacreta, M. Somani, L. Karjalainen, Understanding the impact of grain structure in austenitic stainless steel from a nanograined regime to a coarse-grained regime on osteoblast functions using a novel metal deformation–annealing sequence, Acta Biomater. 9 (2013) 6245–6258.
[294] M. Khajouei-Nezhad, M.H. Paydar, R. Ebrahimi, P. Jenei, P. Nagy, J. Gubicza, Microstructure and mechanical properties of ultrafine-grained aluminum consolidated by high-pressure torsion, Mater. Sci. Eng. A 682 (2017) 501–508.
[295] T. Balusamy, S. Kumar, T.S. Narayanan, Effect of surface nanocrystallization on the corrosion behaviour of AISI 409 stainless steel, Corros. Sci. 52 (2010) 3826–3834.
[296] R.Z. Valiev, Y. Estrin, Z. Horita, T.G. Langdon, M.J. Zechetbauer, Y.T. Zhu, Producing bulk ultrafine-grained materials by severe plastic deformation, Jom 58 (2006) 33–39.
[297] T.G. Langdon, Twenty-five years of ultrafine-grained materials: achieving exceptional properties through grain refinement, Acta Mater. 61 (2013) 7035–7059.
[298] M. El-Tahawy, Y. Huang, T. Um, H. Choe, J.L. Lábár, T.G. Langdon, J. Gubicza, Stored energy in ultrafine-grained 316L stainless steel processed by high-pressure torsion, J. Mater. Res. Technol. 6 (2017) 339–347.
[299] M. El-Tahawy, J. Gubicza, Y. Huang, H.L. Choi, H.M. Choe, J.L. Lábár, T. G. Langdon, The influence of plastic deformation on lattice defect structure and mechanical properties of 316L austenitic stainless steel. Materials Science Forum, Trans Tech Publ, 2017, pp. 13–18.
[300] M. Tikhonova, N. Enikeev, R.Z. Valiev, A. Belyakov, R. Kaibyshev, Submicrocrystalline austenitic stainless steel processed by cold or warm high pressure torsion. Materials Science Forum, Trans Tech Publ, 2016, pp. 398–403.
[301] C. Xu, Z. Horita, T.G. Langdon, The evolution of homogeneity in processing by high-pressure torsion, Acta Mater. 55 (2007) 203–212.
[302] Y.T. Zhu, T.G. Langdon, The fundamentals of nanostructured materials processed by severe plastic deformation, Jom 56 (2004) 58–63.
[303] A. Zhilyaev, G. Nurislamova, B.-K. Kim, M. Baró, J. Szpunar, T. Langdon, Experimental parameters influencing grain refinement and microstructural evolution during high-pressure torsion, Acta Mater. 51 (2003) 753–765.
[304] S. Krishnan, J. Dumbre, S. Bhatt, E.T. Akinlabi, R. Ramalingam, Effect of crystallographic orientation on the pitting corrosion resistance of laser surface melted AISI 304L austenitic stainless steel, Int. J. Mech. Aerosp. Ind. Mechatron. Eng. 7 (2013) 239–242.
[305] X. Lou, M.A. Othon, R.B. Rebak, Corrosion fatigue crack growth of laser additively-manufactured 316L stainless steel in high temperature water, Corros. Sci. 127 (2017) 120–130.
[306] L. Liu, Y. Li, F. Wang, Electrochemical corrosion behavior of nanocrystalline materials—a review, J. Mater. Sci. Technol. 26 (2010) 1–14.
[307] K. Ralston, N. Birbilis, C. Davies, Revealing the relationship between grain size and corrosion rate of metals, Scr. Mater. 63 (2010) 1201–1204.
[308] J. Lippold, W. Savage, Solidification of austenitic stainless steel weldments: part III–the effect of solidification behavior on hot cracking susceptibility, Weld. J. 61 (1982) 388.
[309] A. Kington, F. Noble, σ phase embrittlement of a type 310 stainless steel, Mater. Sci. Eng. A 138 (1991) 259–266.
[310] D. Chastell, P. Flewitt, The formation of the σ phase during long term high temperature creep of type 316 austenitic stainless steel, Mater. Sci. Eng. 38 (1979) 153–162.
[311] X. Chen, J. Li, X. Cheng, H. Wang, Z. Huang, Effect of heat treatment on microstructure, mechanical and corrosion properties of austenitic stainless steel 316L using arc additive manufacturing, Mater. Sci. Eng. A 715 (2018) 307–314.
[312] P. Jerrard, L. Hao, K. Evans, Experimental investigation into selective laser melting of austenitic and martensitic stainless steel powder mixtures, Proc. Inst. Mech. Eng. Part B J. Eng. Manuf. 223 (2009) 1409–1416.
[313] Y. Cui, C.D. Lundin, Austenite-preferential corrosion attack in 316 austenitic stainless steel weld metals, Mater. Des. 28 (2007) 324–328.
[314] G. Suresh, A. Dasgupta, P. Kishor, B. Upadhyay, T. Saravanan, C. Mallika, U. K. Mudali, Effect of laser surface melting on the microstructure and pitting corrosion resistance of 304L SS weldment, Metall. Mater. Trans. B 48 (2017) 2516–2525.
[315] P. Guo, B. Zou, C. Huang, H. Gao, Study on microstructure, mechanical properties and machinability of efficiently additive manufactured AISI 316L stainless steel by high-power direct laser deposition, J. Mater. Process. Technol. 240 (2017) 12–22.
[316] B. Zheng, Y. Zhou, J. Smugeresky, J. Schoenung, E. Lavernia, Thermal behavior and microstructure evolution during laser deposition with laser-engineered net shaping: part I. Experimental investigation and discussionI, Metall. Mater. Trans. A 39 (2008) 2237–2245.
[317] A.F. Padilha, R.L. Plaut, P.R. Rios, Stainless steel heat treatment. Steel Heat Treatment, CRC Press, 2006, pp. 706–751.

[318] O. Salman, C. Gammer, A. Chaubey, J. Eckert, S. Scudino, Effect of heat treatment on microstructure and mechanical properties of 316L steel synthesized by selective laser melting, Mater. Sci. Eng. A 748 (2019) 205–212.
[319] I. Gibson, D.W. Rosen, B. Stucker, Additive Manufacturing Technologies, Springer, 2014.
[320] M. Dodaran, A.H. Ettefagh, S. Guo, M. Khonsari, W. Meng, N. Shamsaei, S. Shao, Effect of alloying elements on the γ'antiphase boundary energy in Ni-base superalloys, Intermetallics 117 (2020), 106670.